Final report for AOARD/ ITC-PAC Grant 114071 "Silica & Germanate Glass High Power Fiber Laser Sources"

Prepared: January 2014

PI and Co-PI information: Principal Investigator: Prof Tanya Monro

Co investigators: A/Prof Heike Ebendorff-Heidepriem, A/Prof David Lancaster, Dr David Ottaway

Institute for Photonics and Advanced Sensing (IPAS),

The University of Adelaide, Australia

Period of Investigation: 2011-2013

Aim of the project:

The research aims of this project were to develop capability in fundamental materials, fabrication techniques, and design of two glass systems that are leading candidates for new fiber laser architectures operating in the 1-4 µm spectral region.

A-1 Investigate fundamental fabrication, design & thermal limitations of silica fibers (2-2.1 µm lasing)

A-2 Establish techniques for improving the pump coupling to fibres via development of air structured claddings (also known as JAC fibres, a form of double clad fibre) at these wavelengths;

A-3 Investigate development of large mode-area cores for higher power operation of fiber lasers.

B-1 Develop techniques for the fabrication and processing of germanate glass fibers to underpin the development of active germanate fibres for fibre lasers

B-2 Explore high temperature variants of germanate glasses for improved fiber lasers

B-3 Demonstrate new forms of germanate fibre lasers for the 2-3.5 µm range using Tm and Ho rare earth dopants.

Executive Summary:

The AOARD funding for the last 3 years has contributed to development of substantive capability at IPAS in all project target areas, and IPAS is well positioned to build on these unique and complementary activities. With the complete relocation of fabrication facilities and fibre manufacturing to new laboratories, 'the Braggs' ($94 M$), we now possess an integrated specialist fiber manufacturing facility. We have achieved a vertically integrated capability in fabricating laser active glasses, designing both microstructured and leaky mode fibre designs, fabricating preforms, drawing fibers, characterizing fiber

Report Documentation Page		*Form Approved* *OMB No. 0704-0188*

Public reporting burden for the collection of information is estimated to average 1 hour per response, including the time for reviewing instructions, searching existing data sources, gathering and maintaining the data needed, and completing and reviewing the collection of information. Send comments regarding this burden estimate or any other aspect of this collection of information, including suggestions for reducing this burden, to Washington Headquarters Services, Directorate for Information Operations and Reports, 1215 Jefferson Davis Highway, Suite 1204, Arlington VA 22202-4302. Respondents should be aware that notwithstanding any other provision of law, no person shall be subject to a penalty for failing to comply with a collection of information if it does not display a currently valid OMB control number.

1. REPORT DATE **25 FEB 2014**	2. REPORT TYPE **Final**	3. DATES COVERED **26-09-2011 to 25-09-2013**
4. TITLE AND SUBTITLE **Silica and Germanate Glass High Power Fiber Laser Sources**		5a. CONTRACT NUMBER **FA23861114071**
		5b. GRANT NUMBER
		5c. PROGRAM ELEMENT NUMBER
6. AUTHOR(S) **Tanya Monro**		5d. PROJECT NUMBER
		5e. TASK NUMBER
		5f. WORK UNIT NUMBER
7. PERFORMING ORGANIZATION NAME(S) AND ADDRESS(ES) **University of Adelaide,School of Chemistry and Physics,Adelaide SA 5005,Australia,NA,NA**		8. PERFORMING ORGANIZATION REPORT NUMBER **N/A**
9. SPONSORING/MONITORING AGENCY NAME(S) AND ADDRESS(ES) **AOARD, UNIT 45002, APO, AP, 96338-5002**		10. SPONSOR/MONITOR'S ACRONYM(S) **AOARD**
		11. SPONSOR/MONITOR'S REPORT NUMBER(S) **AOARD-114071**
12. DISTRIBUTION/AVAILABILITY STATEMENT **Approved for public release; distribution unlimited**		
13. SUPPLEMENTARY NOTES		

14. ABSTRACT

The overarching aims of this project were to develop capabilities in fundamental materials, fabrication techniques, and design of two leading candidate glass systems for new fiber laser architectures operating in the 1-4 µm spectral region. The research involved investigation (1) of fundamental design and thermal limitations of IR silica fibers in the 2-2.1 µm range; (2) of techniques for power handling using air structured cladding; and (3) examination and characterization of Tm+ doped germanate glass fiber lasers that operate in the 2-3.5 µm range. Research accomplishments include 1) successful fabrication of a range of index and microstructured guided rare-earth doped silica fibers using a modified chemical vapor deposition system; 2) development of an air-jacketed 2.1 µm microstructured fiber and fiber laser with demonstrated high quantum efficiency; 3) demonstration of a range of germanate glasses and optimization for laser and non-linear applications; 4) development of extruded germanate microstructured preforms that have been drawn into microstructured optical fibers suitable for laser and non-linear applications; and 5) fabrication of a range of undoped and holmium doped germanate microstructured fibers. Judd-Ofelt modeling was undertaken to estimate branching ratios and emission cross-sections and predict laser performance of rare earth doped germanate glass lasers. Simulations and fabrication of ?leaky-mode? large mode area fibers was also investigated. This research led to development of novel complex microstructured features in a relatively immature glass (especially when compared to silica), whilst maintaining low-loss, and testing the design as a laser in the short to mid-infrared, which is one of the hardest spectral regions to operate a laser.

16. SECURITY CLASSIFICATION OF:			17. LIMITATION OF ABSTRACT	18. NUMBER OF PAGES	19a. NAME OF RESPONSIBLE PERSON
a. REPORT **unclassified**	b. ABSTRACT **unclassified**	c. THIS PAGE **unclassified**	**Same as Report (SAR)**	**40**	

losses, and developing fiber lasers. Over the past 3 years AOARD (contract #114071) has provided a level of funding which has allowed us to steadily grow our germanate and silica fiber laser capabilities. This funding has led towards IPAS possessing unique capability to produce germanate glass, microstructured germanate glass optical fibers, and microstructured rare earth doped silica fibers.

Project Outcome Summary

A-1
a. Installation and completion of a modified chemical vapor deposition system for fabricating silica fibres.
b. Successful fabrication of a range of index guided and microstructured guided rare-earth doped silica fibres.

A-2:
a. Pioneering development of an air-jacketed 2.1 µm microstructured fiber and fiber laser with demonstrated high quantum efficiency.

A-3:
a. Simulations and fabrication of 'leaky-mode' large mode area fibers has been undertaken.

B-1:
a. An extensive program has been undertaken to develop a suite of germanate glasses optimized for a range of applications.

B-2:
a. A range of germanate glasses have been demonstrated and optimised for laser and non-linear applications. To predict laser performance of rare earth doped germanate glass lasers we undertook Judd-Ofelt modeling of these systems to estimate branching ratios and emission cross-sections.

B-3:
a. IPAS has pioneered the development of extruded germanate microstructured preforms which have been drawn into microstructured optical fibers suitable for laser and non-linear applications. A range of undoped and holmium doped germanate microstructured fibers have been demonstrated. The fiber designs were driven by a desire for large mode areas to support high peak power laser operation. Characterisation of the fibers for laser operation is ongoing.

A-1: Silica fiber development:

Progress Achieved:

The contract has seen the completion and the commissioning of our end-to-end silica fibre laser manufacturing facility which includes the construction and recent commissioning of the new dedicated fibre draw tower laboratory at the Thebarton campus of the University of Adelaide (UoA).

Modified Chemical Vapour Deposition (MCVD) based fibre facility

The work conducted to achieve this capability includes further commissioning and refinement of the preform manufacturing laboratory, enhancements to the modified chemical vapour deposition system, and commissioning of an ultrasonic mill for preform drilling and milling.

With the new $3.2M silica preform facility installed in 2010, the initial focus was the production and characterisation of a range of rare earth doped preforms. During this preform development phase we identified and implemented a number of essential modifications to further optimise preform manufacture. As we are the first (to the best of our knowledge) MCVD facility to use on-demand generate hydrogen and oxygen on site (for the high temperature burner), we had to modify the Teledyne hydrogen generator to allow it to operate in the required on-demand fashion as otherwise the
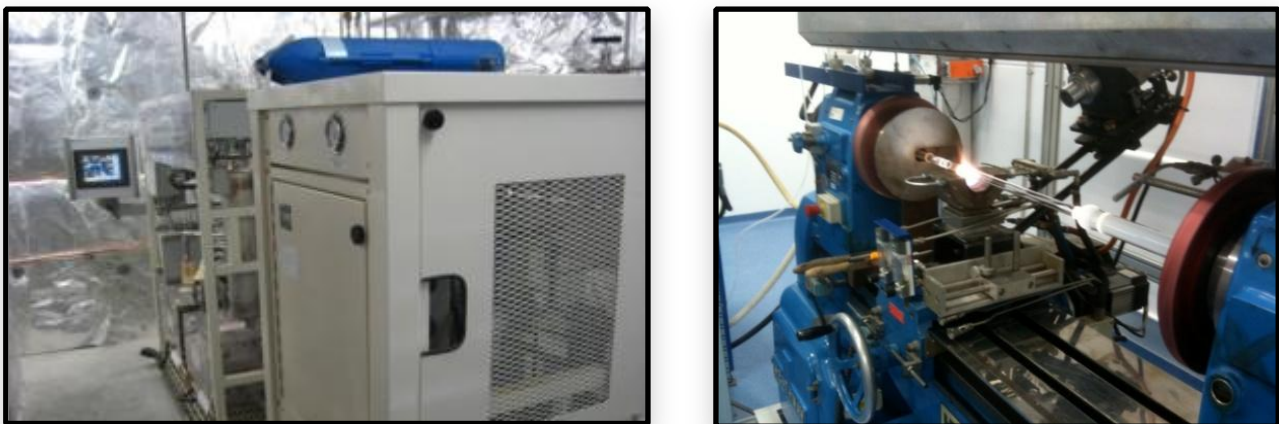
Figure 1(a&b): Photographs of the (a) IPAS on-demand hydrogen/oxygen generator production capability designed to supply the MCVD lathe, and the (b) MCVD lathe in operation

non-steady state requirements of the MCVD burner caused the hydrogen generator to continually trip. The addition of a buffer hydrogen tank in early 2011, alleviated the hydrogen surge requirements and remedied the hydrogen generator trip problem, and allowed the MCVD lathe to operate correctly.

The first quarter of 2011 saw the completion of the $1.5M project to build a dedicated tower laboratory at Thebarton, and final commissioning of our end-to-end silica fibre laser manufacturing facility which

Figure 2: A machined Thulium doped silica preforms prior to drawing into a fibre. The bottom preform has been in-house machined into a hexagonal cross-section to improve pump absorption when operated as a double-clad fibre laser. Both preforms have also had 'handles' attached for easier drawing into fibres.

then allowed us to draw the preforms to fibre and measure their characteristics. As part of the draw tower commissioning we also upgraded the control system to digital (from analogue) which increases the reliability, and allows easier firmware and hardware upgrades in the future. We have now completed manufacture and testing of a range of high performing thulium doped silica fibres that have been demonstrated as functioning fibre lasers. In addition we also commissioned an upgrade of the fibre draw tower from the analogue control system and motors to an all digital system to the drawing capability of the tower.

Our current progress in the preform fabrication area is demonstrated by the production of a series of thulium doped (solution) silica preforms, with several preforms machined into both 'D' and hexagonal structures which are required for drawing into double-clad fibre. These preforms were drawn to fibres by the IPAS silica draw tower. Fig. 1(a,b) shows the IPAS hydrogen generator and MCVD preform lathe, and fig. 2 shows a round and machined thulium doped silica preform, respectively.

A new research topic we are investigating is the use of multiple solution doping steps in order to achieve higher thulium dopant concentrations, which is anticipated to improve fibre efficiency (IPAS #4, #5 – described later).

Fig. 2 shows a typical refractive index of profile of a rare-earth solution doped preform. The starting silica tube can be seen (r=2.5 to 10mm), a depressed region made by multiple deposition layers of silica (r~1 to 2.5mm), and the high refractive index guiding core made up of solution doped aluminosilicate and rare earth

**Fibre draw tower facility (Thebarton Campus of the UoA)**
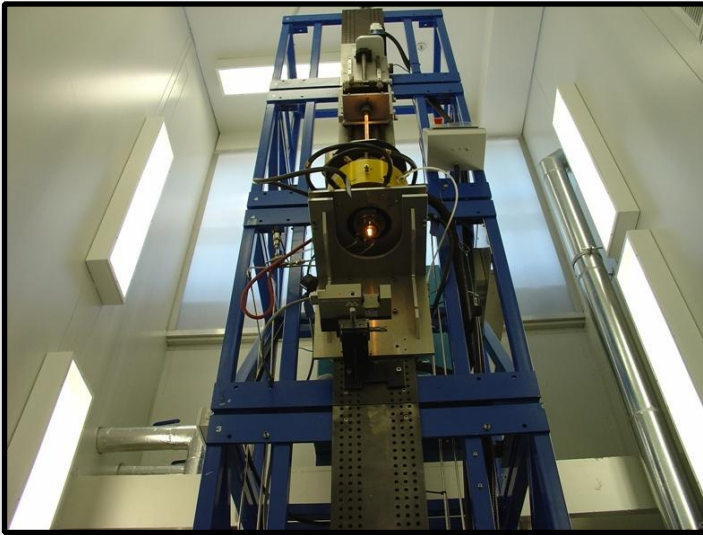
Figure 4: Photograph of the recently commissioned 6 m Heathway silica draw tower operating.
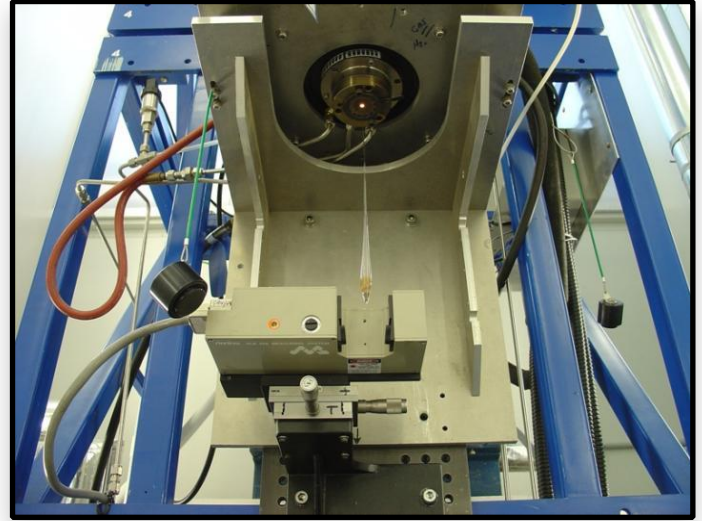
Figure 5: Initial preform melt initiates the fibre draw. The silica glass 'drop-off' can be seen emerging from the furnace and about to pass through the diameter measuring gauge.

Figure 8: Upgraded all-digital draw tower control unit, which was installed during commissioning.
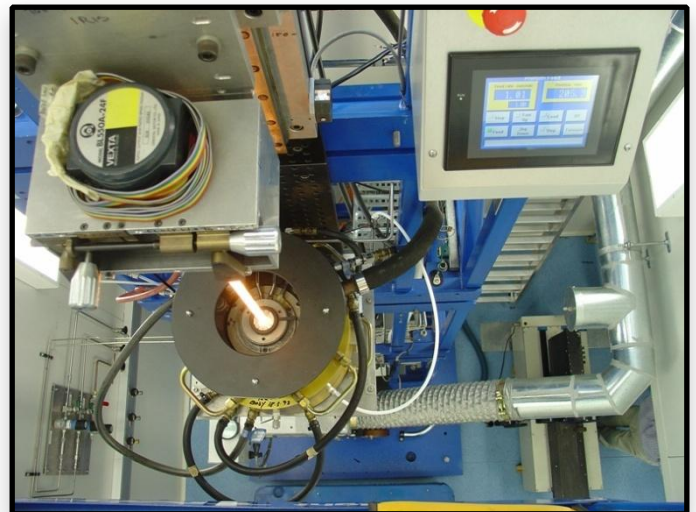
Figure 7: View from the top of the draw tower at the preform feeding into the furnace.

A.2: air-jacketed 2.1 μm microstructured fiber and fiber laser

Silica work component 2: The development of high power fiber silica lasers based on holmium doping

Specific focus of this research over this project has been towards a large mode area air-jacketed double-clad fiber. This involves work in the following areas:

1. Fabricating more versatile depressed cladding geometries in fibers
   a. Specifically we are developing processes to realise high Δn alumino-silicate pedestals in the fibres which allows more flexibility in modal design.
   b. We are taking this approach as the standard technique which uses germanosilicate as a pedestal has drawbacks such as a low achievable Δn, and it introduces high stress into the fiber.
2. Improvements in the NA of the air-jacketted holmium doped fibers.
3. Development of a higher power 1945 nm pump laser to fully characterise the holmium fiber laser

Results and Discussion:

Silica work component 1: Development of depressed cladding structures for large mode area operation

The results shown in Fig. 1 summarise our work in development of alumino-silicate outer cores to realize a high refractive index pedestal. This result is based on fabrication of 3 silica preforms (via modified chemical vapor deposition) where solution doping was used to introduce aluminum to the silica matrix, thus resulting in the formation of an alumino-silicate glass with a higher refractive index. This work allows us to optimize the process to realize arbitrary pedestal heights. In addition to standard solution doping, we are also investigating in-situ solution doping which allows convenient deposition of many layers to realize large pedestal widths. This contrasts with standard solution doping in that the preform does not have to be removed from the lathe to introduce each solution doped layer.
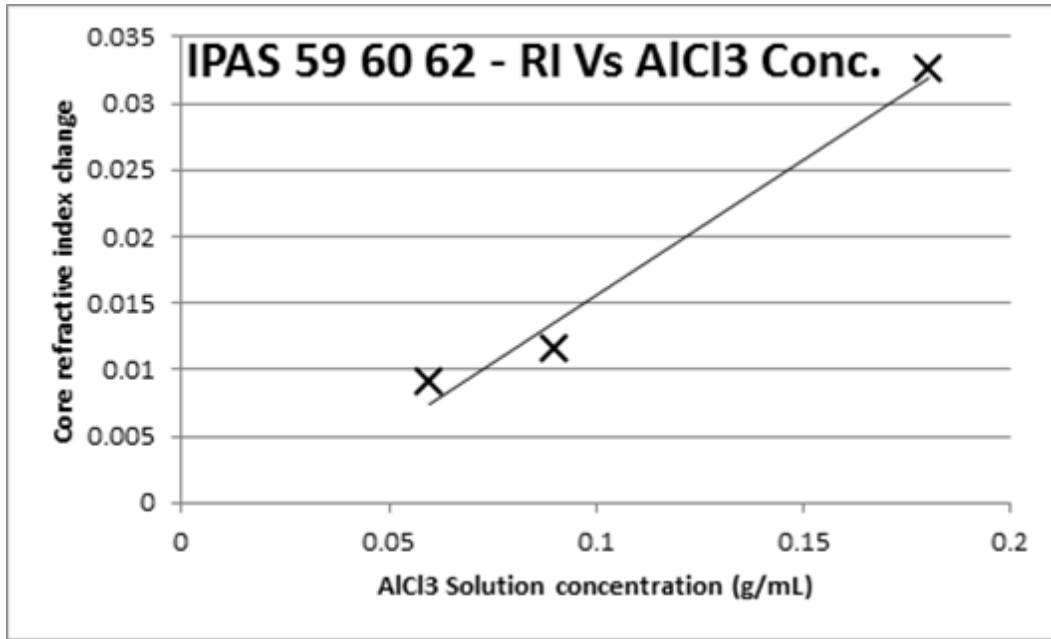
Fig. 1. Measured core refractive index as a function of aluminum chloride solution concentration for 3 different preforms.

Shown in Fig. 2 is an optical microscope image of a holmium doped air-jacketed microstructured double-clad fiber we fabricated. Overlaid on this image are measurements of the core size as well as the strut size which is a critical parameter with regard to increasing the numerical aperture (or acceptance angle) of the fibre.
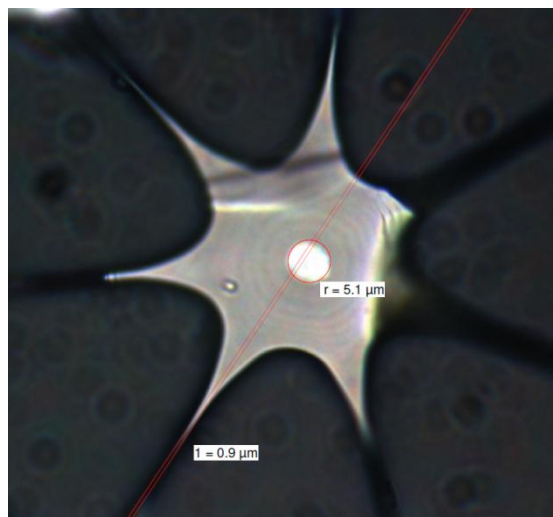

Fig. 2: Optical microscope image of the inner cladding of a holmium doped air-jacketted double-clad fiber.

Shown in Fig. 3 is a measurement of the NA of the fiber as a function of strut thickness which shows the importance of achieving narrow struts for high NA. This parameter is controlled by precisely controlling the preform temperature and active internal pressurisation of the preform during the fiber drawing process.
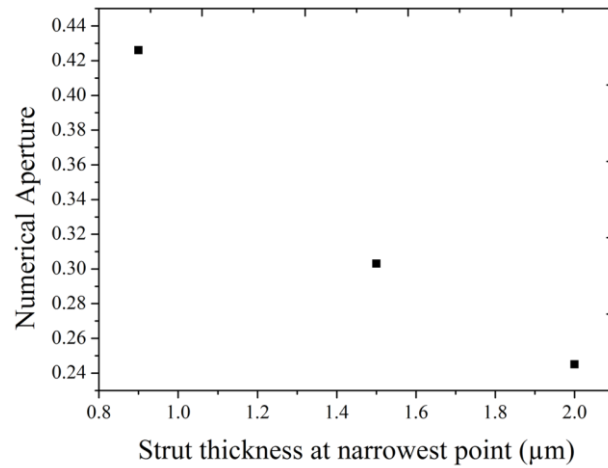
Fig. 3: Measured NA of a holmium doped air-jacketted fiber as a function of strut thickness.

Air-Clad Holmium fiber Laser

Summary

We report the first air-jacketed holmium fibre laser. The laser operates at 2.1 µm with an internal slope efficiency of 69%, and is in-band pumped with a 1.94 µm thulium fibre laser.

I. INTRODUCTION

Holmium emission at 2.1 µm is advantageous for frequency conversion into the mid-infrared, atmospheric transmittance and high-power diffraction limited light generation. The mechanical strength and high melting point of silica make it the ideal host for high power fibre laser applications. However, its infrared vibrational absorption band results in significant attenuation above 2.1 µm [1]. This property has allowed holmium to be the longest wavelength rare-earth doped silica fibre laser.

Power scaling of robustly single-mode rare-earth fibre lasers can be limited by the onset of stimulated Raman scattering in broadband lasers and stimulated Brillouin scattering for narrow linewidth lasers [2]. These non-linear effects scale with intensity in the core, and device length. As the core area for single-mode confinement scales with wavelength, holmium should provide the largest robustly single-mode cores for silica fibre lasers.

A second limitation for power scaling is thermal load. The heat addition of the fibre due to lasing operation is related to the energy defect between the pump and lasing wavelengths. Holmium may be pumped by conventional diodes at 1.15 µm [3], however in-band pumping by direct excitation of the $^5I_7$ energy level at 1.9 µm is the most attractive option due to low thermal heating based on the high stokes efficiency. High-power, low-cost diodes are not available at this wavelength, hence the $^5I_7$ level is commonly tandem-pumped with thulium fibre lasers [4,5,6]. These two common pumping regimes for holmium are shown in Fig. 1.
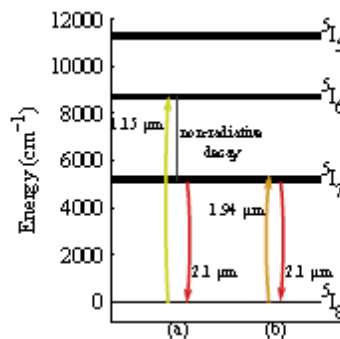
Figure 1 – Simplified energy level diagram of trivalent holmium ion showing transitions for (a) 1.15 µm, and (b) 1.94 µm pumping regimes [7].

The majority of in-band pumped holmium fibre lasers have relied on core-pumping architectures due to absorption of the pump-wavelength by the low refractive index polymers conventionally used as an outer cladding for double-clad thulium fibre lasers. However, the

absorption of the pump wavelength by the polymer cladding not only results in a significant drop in device efficiency, but also acts to reduce the potential for power scaling as polymers have a relatively low thermal failure limit. For this reason the development of high power ytterbium fibre lasers has shifted away from polymer cladding [8,9]. The primary alternatives are highly fluorine-doped outer-claddings and air-jacketed fibre. The former can be fabricated by over-jacketing silica preforms with commercially available fluorine-doped silica tubes to typically achieve cladding numerical apertures (NAs) of 0.28 [9]. Recently, double-clad holmium fibre lasers have been demonstrated with low-index fluorine-doped silica cladding [10]. Air-jacketing has demonstrated NAs up to 0.88 [11]. Although the transition from core-pumped to cladding-pumped devices allows a significant increase in pump power, the reduction in pump absorption for a fixed core results in a longer cavity. The silica losses at the emission wavelength and the onset of non-linear effects restrict the length of holmium fibres for efficient high power applications [1,2]. In addition, the absorption cannot be raised by increasing the dopant concentration due to ion-clustering impacting the efficiency [12]. Hence, a low cladding to core ratio, high NA clad architecture should allow the optimum trade-off between efficiency and power scaling. This work represents the first demonstration of a double-clad, air-jacketed holmium fibre laser; moreover the design is consistent with the aforementioned requirements.

II. FIBRE MANUFACTURE

A 7-hole air clad holmium doped silica fibre was produced by fabricating a step index holmium-doped core preform inside a silica tube using a modified chemical vapour deposition (MCVD) process. The core was solution doped with a high aluminium chloride to holmium ratio to provide a high index core while reducing clustering of the holmium ions that would lead to a reduction in efficiency [12]. The strongly guiding core was chosen to allow characterization of the new fibre geometry without significant bend-induced confinement loss. The refractive index profile of the preform is shown in Fig. 2. This preform was then over-jacketed to increase the cladding diameter for structural stability and ease of handling. A 100 mm section was separated from the 200 mm long preform and the 7-hole cladding was drilled with a 2.8 mm diameter drill (1 mm/min) and a 20 kHz ultrasonic frequency (Sonic-Mill[TM] S10 ultrasonic mill). The holes were centred on a 6 mm diameter ring around the core, to closely surround the ultra-pure MCVD deposited glass which formed the inner-cladding. This maintained a uniform density of glass surrounding the holes, thus preventing uneven expansion during fibre drawing and limiting the guiding region of the inner clad to the high purity, low water content deposition layers. High purity cladding is required due to the OH⁻ absorption in silica at the 1.94 μm holmium pump wavelength [13]. The thickness of the deposited glass was tailored for a low core to inner-cladding area ratio to increase pump absorption and reduce device length.
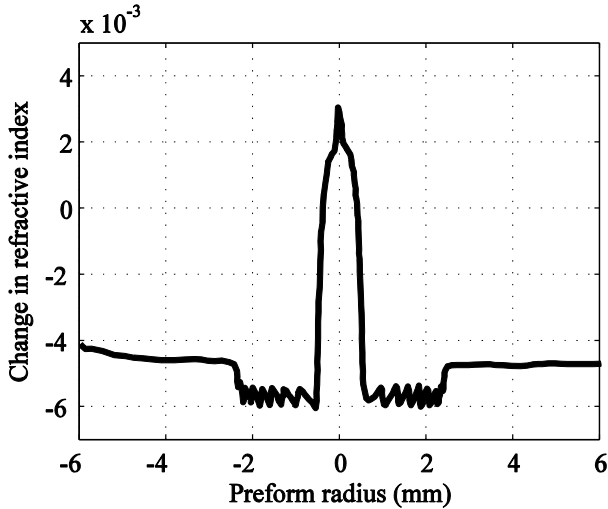
Figure 2- Holmium doped preform refractive index profile

The fibre was drawn using active pressurisation of the preform to control the expansion of the holes. The resultant fibre had a core diameter of 10 µm, an inner cladding diameter of approximately 30 µm, and an outer diameter of 185 µm as shown in Fig. 3. In this initial fibre draw, the resultant strut thickness was larger than desired at ~2 to 3 µm, which is expected to limit the achievable inner cladding NA [11]. The fibre was then coated with a high-index polymer coating for structural stability. The fibre was found to have high mechanical strength, and could be easily cleaved using non-specialized fibre cleavers. This is unsurprising because of the large glass outer cladding and the resultant small change of 5.97×10^7 mm^4 to 5.54×10^7 mm^4 in the second moment of area of the fibre cross-section from a solid circular fibre. Additionally, the fracture of fibres is often caused by the propagation of micro-cracks initiated by surface defects. This fibre design positions the holes close to the centre of the fibre which is close to the neutral axis when the fibre is stressed due to bending, reducing the stress around the drilling defects.
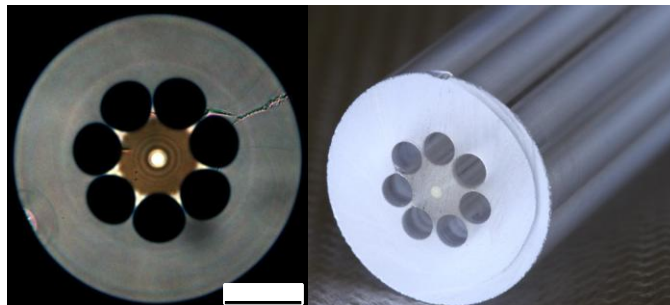
Figure 3 – Images of the air clad, holmium doped fibre (left) and preform after drilling (right).
   Drilling enables the rapid development of research fibres, in particular the investigation of novel internal fibre geometries produced using an MCVD lathe. Direct drilling of the preform eliminates HF etching of the outer cladding required for stacking as the air-cladding may be drilled in any position within the preform surrounding the desired features.

III.   Fibre Characterisation

Spot and broadband cutback measurements were performed by pumping the inner-cladding (region surrounded by holes) of the fibre with a thulium fibre laser and probing with a white light source (WLS). The loss in the holmium absorption band at 1.94 μm was measured as 1.4 dB/m in the inner cladding. Broadband loss spectra obtained with a super-continuum source and a Yokogawa AQ6375 optical spectrum analyser indicated a strong absorption of 1.4 dB/m at 1.4 μm, which is consistent with water contamination. The source of this contamination was identified as a fault in the chlorine flow regulator. This occurred during the production of this preform, reducing the effectiveness of the drying stage.

The divergence of the cladding was estimated for a 50 mm section of fibre. A 1.53 μm fibre laser was used to prevent core absorption preferentially absorbing higher order modes and this was coupled into the inner cladding using a 0.56 NA microscope objective. The resultant NA of the inner cladding was found to be 0.25. This relatively low result was expected due to the struts of the air cladding having greater thickness than half the wavelength [11].

IV.   Laser configuration

The laser performance of the fibre was characterized in a low-power single-pass pump configuration shown in Fig. 4. The fibre was pumped by a single-mode thulium fibre laser operating at 1.95 μm. The power of the pump was monitored using the front face reflection of a wedge in the collimated beam that was calibrated to the transmission of the wedge. The pump beam was launched into the inner-cladding of the fibre laser by use of a f = 30 mm lens. The laser cavity was bounded by an input highly reflective (HR) dichroic at 2.05 μm and the Fresnel reflection at the output end of the fibre. The laser output was separated from the pump using an angled dichroic filter HR at 1.95 μm, partially reflective at 2.05 μm, and the output power was calibrated to the transmission of filter. The lasing performance versus length of the fibre is shown in Fig. 5.
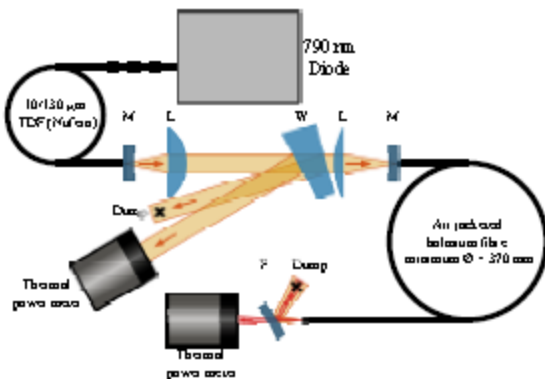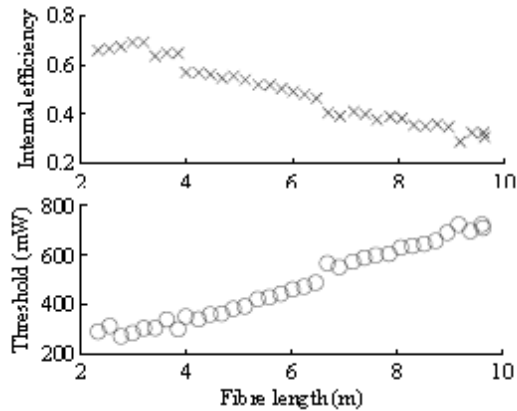

Figure 4 - Laser cutback configuration

Figure 5 – Laser performance of absorbed pump to calibrated output versus length.

In this configuration a maximum slope efficiency of the calibrated output to absorbed pump of 69% was achieved with a 300 mW threshold. This corresponded to a resonator length of 3.2 m. The calibrated output power versus absorbed power for this length is shown in Fig. 6. We expect that this performance was compromised by the high OH⁻ content we measured in the fibre core. A maximum output of 900 mW was measured with a 3.8 m cavity and was limited by the pump power of the laser used for characterisation.
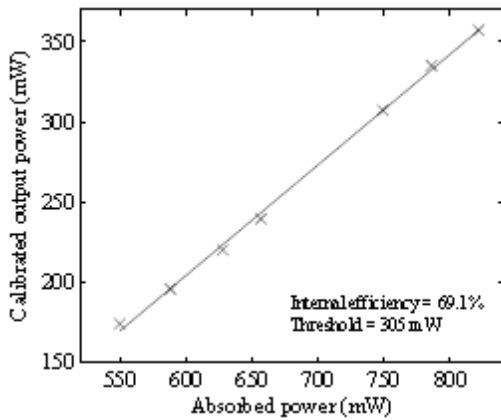
Figure 6 - Calibrated output power versus absorbed pump at a 3.2 m cavity length.

The output spectrum of the fibre laser was measured with the Yokogawa AQ6375 OSA and is shown in Fig. 7. Beam quality measurements are still to be performed. However imaging of the fibre output, inset in Fig. 7, suggests single trasverse mode operation consistent with the core V-number of 2.4 (the NA is based on the preform refractive index of 0.15). Optimisation of this fibre geometry should provide the basis for a new class of high power holmium fibre lasers.
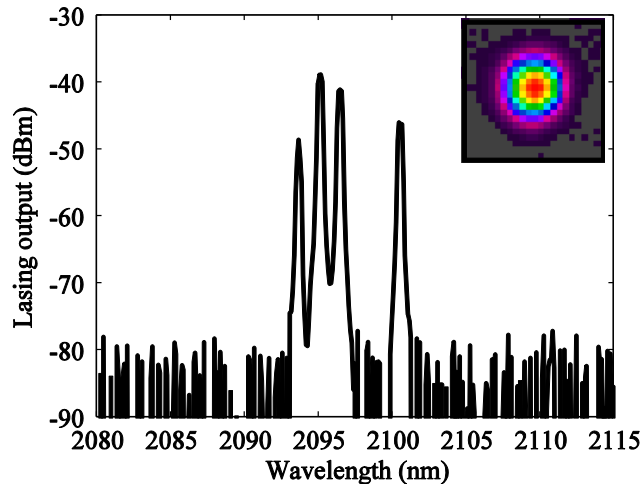
Figure 7 - Output spectrum of the fibre laser. Inset: Typical beam profile.

V. CONCLUSION

In conclusion we have demonstrated that use of a high NA air-jacket cladding and low NA core, along with a small cladding to core area ratio, is thus ideal for efficient diffraction-limited holmium fibre laser operation.

This research represents the first step in the development of holmium-doped, air-jacketed fibre lasers, and we consider that the internal slope efficiency of 69% validates this approach.

VI. REFERENCES

[1] Kurkov, A. S., Sholokhov, E. M., Tsvetkov, V. B., Marakulin, V., Minashina, L., Medvedkov, O. I., & Kosolapov, F.. 'Holmium fibre laser with record quantum efficiency', IEEE J. Quantum Electron., 41(6), 492-494, (2011)

[2] Dawson, J. W., Messerly, M. J., Beach, R. J., Shverdin, M. Y., Stappaerts, E., Sridharan, A. K., Pax, P. H., et al.. 'Analysis of the scalability of diffraction-limited fiber lasers and amplifiers to high average power', Opt Exp., 16(17), 13240-66, (2008)

[3] Jackson, S. D., Bugge, F., & Erbert, G., 'Directly diode-pumped holmium fiber lasers', Opt. lett., 32(17), 2496-8, (2007)

[4] Jackson, S. D. 'Mid-infrared Holmium Fiber Lasers. IEEE J. of Quantum Electron', 42(2), 187-191, (2006)

[5] Wu, K. S., Ottaway, D., Munch, J., Lancaster, D. G., Bennetts, S., & Jackson, S. D., 'Gain-switched holmium-doped fibre laser', Opt. Exp., 17(23), 20872-7, (2009)

[6] Hollitt, S., Simakov, N., Hemming, A., Haub, J., & Carter, A.. 'A linearly polarised, pulsed Ho-doped fiber laser', Opt. Exp. 20(15), 16285-16290, (2012)

[7] Gruber, J. B., Hills, M. E., Seltzer, M. D., Stevens, S. B., Morrison, C., Turner, G., & Kokta, M. R.. Energy levels and crystal quantum states of trivalent holmium in Yttrium aluminum garnet', J. of Appl. Phys., 69(12), 8183, (1991)

[8] Stutzki, F., Jansen, F., Eidam, T., Steinmetz, A., Jauregui, C., Limpert, J., & Tünnermann, A., 'High average power large-pitch fiber amplifier with robust single-mode operation', Opt. Lett., 36(5), 689-691, (2011)

[9] Dong, L., McKay, H., Fu, L., Ohta, M., Marcinkevicius, A., Suzuki, S., & Fermann, M. E.. 'Ytterbium-doped all glass leakage channel fibers with highly fluorine-doped silica pump cladding', Opt. Exp, 17(11), 8962-9, (2009)

[10] Hemming, A., Bennetts, S., Simakov, N., Haub, J., & Carter, A., 'Development of resonantly cladding-pumped holmium-doped fibre lasers', Proc. SPIE, 8237, 82371J-82371J-9. (2012)

[11] Wadsworth, W., & Percival, R., 'Very high numerical aperture fibers' IEEE Photon. Tech. Lett. 16(3), 843-845, (2004)

[12] Kurkov, A. S., Sholokhov, E. M., Marakulin, V., Minashina, L.A., 'Effect of active-ion concentration on holmium fibre laser efficiency'. IEEE J. Quantum Electron., 40(5), 386-388, (2010)

[13] Humbach, O., Fabian, H., Grzesik, U., Haken, U., & Heitmann, W. 'Analysis of OH absorption bands in synthetic silica', J. of Non-Crystal. Solids, 203, 19-26, (1996)

A-3: Simulations and fabrication of 'leaky-mode' large mode-area fibers

Modelling and Fabrication of a Leaky Mode Depressed Clad Ho^{3+} Fiber

Abstract: This work is an investigation of mode suppression in leaky mode fiber lasers. We present modelling and fabrication details for a depressed cladding holmium doped silica fiber.

1. Introduction

Power scaling of single frequency and pulsed fiber lasers are limited by the onset of non-linear effects. The threshold for these effects can be raised by reducing the length of a fiber laser or by increasing its core area. However, this can result in the propagation of higher order modes (HOM) that reduce output beam quality. Recently large pitch fibers have shown promise for single mode, large mode area fiber lasers by providing fundamental mode confinement, while allowing HOMs to leak from the core [1]. This paper reports on the modelling and fabrication of a leaky mode, depressed clad architecture that will allow the investigation into cladding confinement of leaky modes without the considerable manufacturing complexity of a microstructured large pitch fiber.

2. Fiber manufacture

The depressed cladding fiber was manufactured in-house using modified chemical vapour deposition, solution doping, and a silica fiber draw tower. A low Ho^{3+} concentration was chosen to allow core pumping which also results in improved laser performance due to low ion clustering [2]. The addition of Ho^{3+} was found to reduce the core refractive index which was compensated by tailoring the concentration of AlCl$_3$ in solution. A ring surrounding the core was then doped with BBr$_3$ to produce the depressed inner cladding. The refractive index profile of the preform and a microscope image of the fiber profile are shown in Fig. 1. The preform was then drawn to a fiber with a 15 µm core radius and a 500 µm outer cladding.
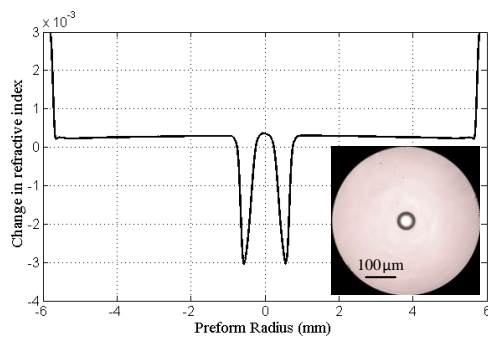

Fig. 1. Refractive index profile of the fiber preform averaged over preform length (PK2600). Inset: Microscope image of fiber face with a 15µm core radius.
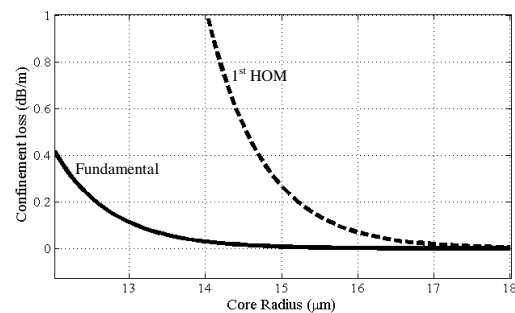

Fig. 2. Waveguide confinement modelling as a function of core radius of the fundamental (solid) and first HOM (dashed) of the depressed cladding fiber.

3. Confinement modelling and laser setup

The refractive index profile of the optical fiber was approximated as a three ring step index fiber with infinite outer cladding and the leakage from the core to outer cladding was calculated by directly solving Maxwell's equations [3]. Fig. 2 shows the modeled loss for the fundamental and first HOM. When operating in a laser cavity this should provide preferential gain for the fundamental mode, thus achieving lowest order mode operation. This fiber is now being characterised in a 1944 nm Tm^{3+} fiber laser tandem pumped, 2.1 µm laser configuration.

With Ho^{3+} lasers near 2.1 µm being the longest wavelength silica fiber lasers, the geometric scaling of the core for single mode guidance should provide the largest achievable mode areas in silica fiber architectures. This makes Ho^{3+} an attractive gain medium for investigating power scaling in leaky mode fiber lasers.

4. References

[1] F. Stutzki, F. Jansen, T. Eidam, A. Steinmetz, C. Jauregui, J. Limpert, and A. Tünnermann, "High average power large-pitch fiber amplifier with robust single-mode operation" *Optics Letters* **36**(5), 689-691 (2011)

[2] A.S. Kurkov,, E.M. Sholokhov, A.V. Marakulin and L.A. Minashina, "Effect of active-ion concentration on holmium fiber laser efficiency" *Quantum Electron* **40**, 386-388 (2010).

[3] S. Warren-Smith, "Fluorescence-based chemical sensing using suspended-core microstructured optical fibres" PhD thesis, Univ. of Adelaide (2010).

B-1, B-2, B-3: Germanate glass and fiber development

2011-2012

Background and project aims

While silica-based fiber lasers undeniably offer access to kW power levels, they cease to be transparent beyond about 2.1µm, and other materials are required to access this wavelength range. Access to the mid-infrared spectral region can be provided by the use of mid-infrared transmitting "soft" glass such as those under development at the University of Adelaide. Truly high power operation (>100W, say) cannot be envisaged with mid-infrared transmitting soft glass-based fiber lasers principally because the glasses considered to date (chalcogenide, tellurite, fluoride, etc), suffer from low damage thresholds due to low thermal stability of the glasses.

Germanate glasses are an appealing and as yet relatively unexplored alternative choice for the fabrication of high power fiber lasers. The combination of reasonable thermal properties (relative to soft glasses) and relatively low phonon energy (relative to silica glass) make these glasses attractive for high power laser operation in the wavelength range 2-3 µm, i.e. the short-infrared.

High power operation at 2 µm will allow a route to efficient pumping of non-linear fiber optic systems for extending further into the mid-infrared. The aim of this proposal is to develop initial germanate fiber lasers operating at 2 µm and 2.1 µm using Tm^{3+} and Ho^{3+} as the active laser ions, respectively. The softening point of the glass is sufficiently low that current soft-glass extrusion techniques can be used to fabricate new high efficiency laser geometries. This offers advantages not currently available to silica fiber lasers in that it allows the formation of micro-structured fiber geometries that cannot be made in any other way.

To develop germanate-glass based fiber lasers at ~2 µm it is first necessary to demonstrate the fabrication of low-loss Tm and Ho-doped germanate glasses and simple fibers. We considered two germanate glass systems:

- Low-softening-point germanate glasses that can be extruded using our low-temperature extrusion machine and expertise in complex oxide glass preform extrusion. In addition, these glasses can be drawn using our soft glass drawing tower and building on our experience with drawing microstructured soft glass fibres.
- High-softening-point germanate glass that is commercially available from Kigre Inc and promises higher power operation compared with low-softening-point germanate glasses. A further advantage is that detrimental nonlinear effects such as Raman scattering will be reduced. The high softening point of this germanate glass means that it can only be extruded using our high-temperature extrusion machine, which is scheduled to be installed within this project.

Progress achieved

Capability installation

Controlled-atmosphere high-temperature glass melting capability

The development of new glasses for fibre laser application at and beyond 2µm, low water content in the glass is critical. IPAS was awarded funding for the installation of a controlled-atmosphere high-temperature glass melting facility, which enables melting of germanate glasses under dry atmosphere to reduce the water content. This capability was commissioned in Aug 2011, and has been used to melt glasses developed within this project year under controlled atmosphere conditions. It was subsequently shifted to the IPAS Braggs 'state of the art' laboratory in the first half of 2013.

High-temperature extrusion machine

Under this project a high-temperature extrusion machine, required for the extrusion of preforms from the high-softening-point germanate glass, was acquired from Kigre Inc. The extrusion rig was successfully installed in April 2011, and subsequently moved to the new IPAS building in March 2013. The high-temperature furnace, which will enable extrusion temperatures up to 1400°C, has also now been commissioned.

Glass fabrication and development

Under this project we investigated three types of low-softening-point germanate glasses:

    (a) Commercial bismuth-germanate glass from Schott

    (b) bismuth-germanate glasses developed in-house

    (b) lead-germanate glasses developed in-house

(a) Commercial bismuth-germanate glass from Schott

We acquired billets of 30mm diameter and 15mm length of low-softening germanate glass from Schott. From one billet, we successfully extruded a 10mm diameter rod with excellent surface quality (Fig. B.2). The rod was successfully drawn into a bare, unstructured fiber. The loss spectrum of this fiber was measured using standard cut-back method and a white light source. The loss of the fiber is equal to the bulk glass loss provided by Schott within loss measurement error (Fig. A.2). This demonstrates the potential of this glass for the fabrication of fibers whose loss is only limited by material loss. The fiber loss is 0.4 dB/m at 1.3µm, which is acceptable for short fiber laser applications. The material itself has appreciably higher loss at 2.0µm and 2.4µm due to high water content as a result of large scale glass manufacture.
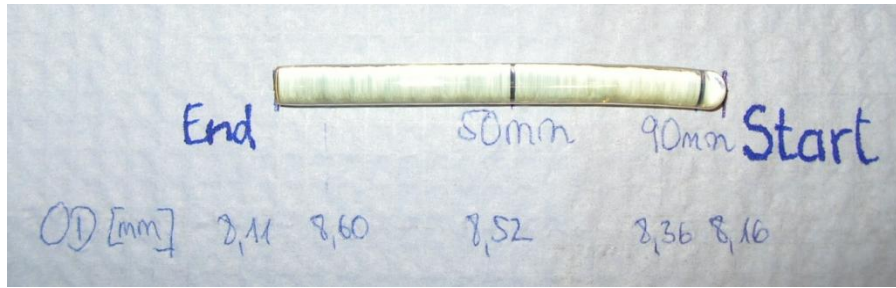
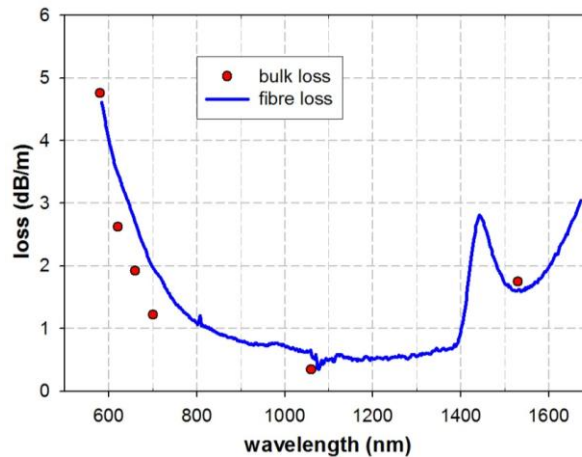*Figure A.1: Photograph of our first extruded rod (2011) using Schott germanate glass (2011).*

Figure A.2: Loss of bulk glass and the first extruded unstructured fiber of Schott germanate glass.

The Schott glass could successfully remelted into a glass using 1250°C melting temperature. However, the first two remelting trials (using different mould materials) resulted in a dark brown glass, whereas the as-received glass has a light yellow colour (Fig. A.3). Glasses with high bismuth oxide content are know to suffer from reduction of the Bi^{3+} to Bi^{0}, whereby the latter forms nanoparticles with a brown colour. For bismuth borosilicate glasses, CeO$_2$ is added to prevent Bi^{3+} reduction. Hence, for the next remelting trial, we added 0.1wt% of CeO$_2$ to the glass, which resulted in a glass with orange colour (Fig. A.3), demonstrating that CeO$_2$ is also suitable to prevent Bi^{3+} reduction in germanate glass. It also shows that more than 0.1wt% CeO$_2$ is required to completely prevent the Bi^{3+} reduction.
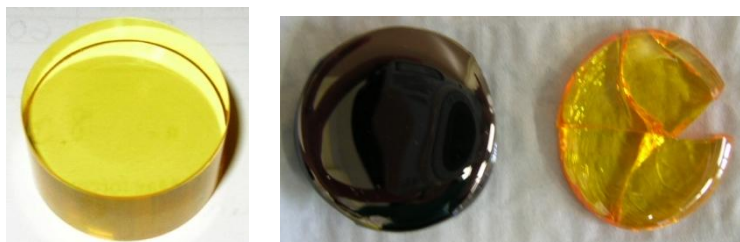
Figure A.3: Photographs of Schott germanate glasses: (left as-received, (mid) remelted without CeO$_2$, (right) remelted with 0.1wt% CeO$_2$.

Using FTIR spectroscopy, we measured the shape and intensity of the hydroxyl (OH) group absorption band at ~3µm (This band is often also referred to as water absorption) (Fig. A.4). The loss of this absorption band is proportionally to the OH content and thus serves as a relative measure for the OH content of a glass. The OH content could be reduced via remelting. For both the as-received and remelted glass (without CeO_2) the IR edge is located at ~3.5µm. This is at a relatively short wavelength compared to germanate glasses, whose IR edge is usually located at 4-5µm. (see also results on in-house lead-germante glasses). This suggests that the Schott glass contains SiO_2 and/or B_2O_3, both components exhibit high phonon energy, which shifts the IR edge towards shorter wavelengths.
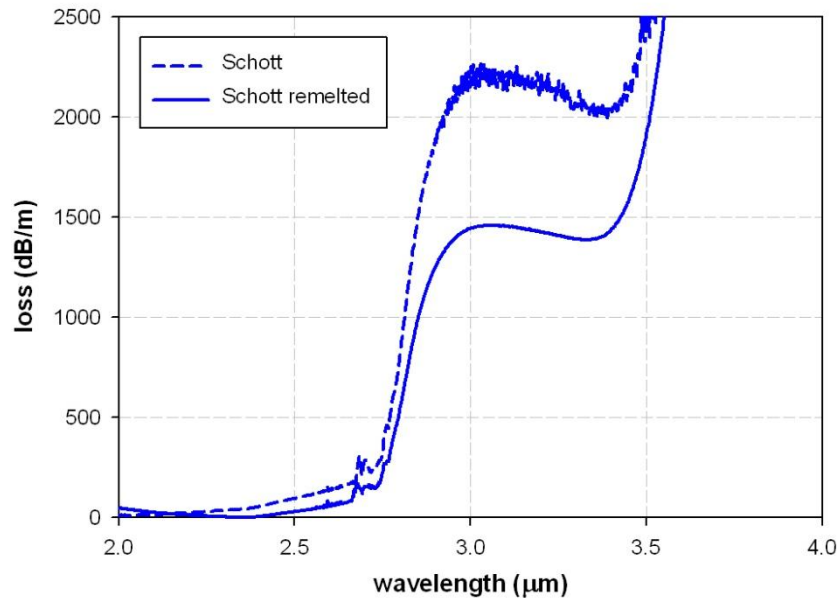
Figure A.4: FTIR spectra of as-received and remelted Schott glasses showing the OH-absorption peak at 2.9 µm and the IR edge at ~3.5µm.

To determine the composition of the germanate glass, we conducted energy dispersive X-ray spectroscopy of the as-received and remelted Schott glass. Note that with this method B_2O_3 cannot be detected. Both samples showed the same glass composition within the relatively large measurement error of >10mol%. The approximate composition of the Schott glass was found to be 34 GeO_2 – 30 Bi_2O_3 – 13 ZnO – 12 SiO_2 – 7 BaO – 4 $(La,Ce)_2O_3$. The presence of SiO_2 correlates with the short wavelength IR edge of the Schott glass.

To test the suitability of the Schott germanate glass for complex preform extrusion, we selected a target preform structure with 1 ring of 6 holes around the core region and a die design used for complex preform extrusion previously. As the glass billets received from Schott have only a small volume, the target preform diameter was only 8mm. Two germanate glass billets were successfully extruded into preforms with 6 holes (Fig. A.5). However, the preforms show a gradual increase of tiny bubbles within the preform from the start to the end of extrusion. These bubbles are assumed to correlate with the tendency of the glass for Bi^{3+} reduction. The same tiny bubble formation was observed for a Schott lead-

silicate glass with high PbO content. As for Bi^{3+}, Pb^{2+} can be easily reduced to Pb^0 in glasses with high PbO content.
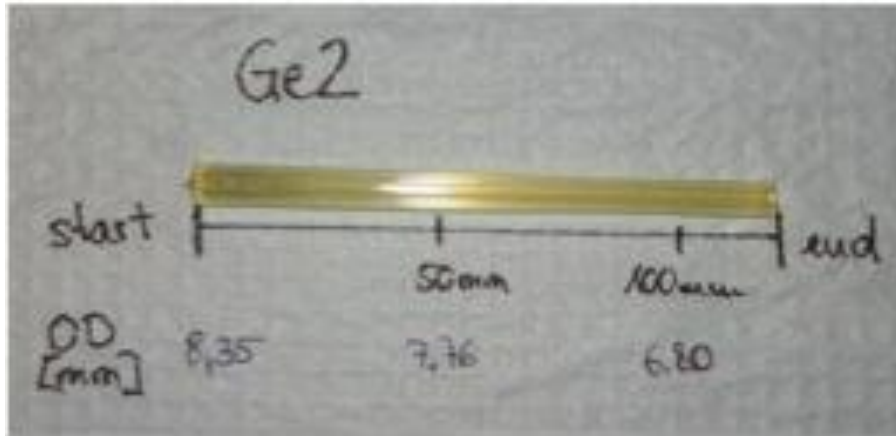

Figure A.5: Photograph of the first extruded preform with 6 holes using Schott germanate glass.

(b) Bismuth-germanate glasses developed in-house

Within the bismuth germanate system, we first explored the glass forming region in the system germanium oxide – bismuth oxide – tungsten oxide on the basis of the results by Yamazaki *et al.* [4] (Fig. A.6). Tungsten oxide was chosen as a third component to increase the crystallization stability and the mechanical strength.
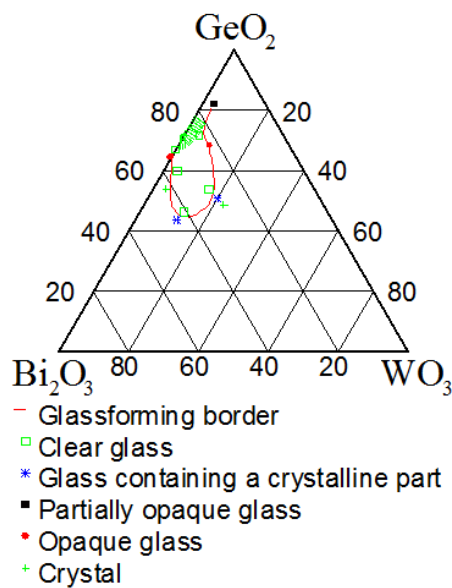
Figure A.6: GeO_2 – Bi_2O_3 – WO_3 system and glass forming region.

A range of glass compositions was melted (Table A.1), and the glass samples were classified into glass forming (a transparent glass can be formed), devitrification (two amorphous non-mixable phases are

formed) and crystallization (the glass melt crystallized while cooling or non melted residuals are found in the glass). First glasses made showed a dark-brown color (Fig. A.7), similar to the first remelted Schott bismuth-germanate glasses, which is attributed to Bi^{3+} reduction to Bi^0. As for the Schott glass remelting, we added 0.1-0.5 mol% CeO_2 to the raw material batch, which resulted in a yellow glass (Fig. A.9). As the next step, the glasses were doped with an additional 0.5 wt% of Tm_2O_3.

Figure A.7: Photographs of 70 GeO_2 – 25 Bi_2O_3 – 5 WO_3 glasses without CeO_2 (left) and with 0.1 CeO_2 substituted for GeO_2 (right).

Table A.1: Melted glass compositions in the multicomponent system GeO_2-Bi_2O_3-WO_3 and classification and evaluation of the glass forming ability.

GeO_2	Bi_2O_3	WO_3	CeO_2	Tm_2O_3	classification
55	39,5	5	0,5	0,3	a
55	34,5	10	0,5	0,3	b
60	34,5	5	0,5	0,3	a
65	10	20	0	0	c
69,9	25	5	0,1	0	a
70	25	5	0	0	a
70	24,5	5	0,5	0,3	a
75	19,5	5	0,5	0,3	a
80	14,5	5	0,5	0,3	c

a-glass forming, b-devitrification, c-crystallization

Compositions of the multi-component system that formed a glass were analyzed with differential scanning calorimetry (DSC) to find out the glass transition temperature T_g and onset of glass

crystallization T_c. These temperatures guide the choice of annealing, extrusion and fiber drawing temperatures. Figure A.8 shows a DSC curve for a 55 GeO_2 – 39.5 Bi_2O_3 – 5 WO_3 glass.
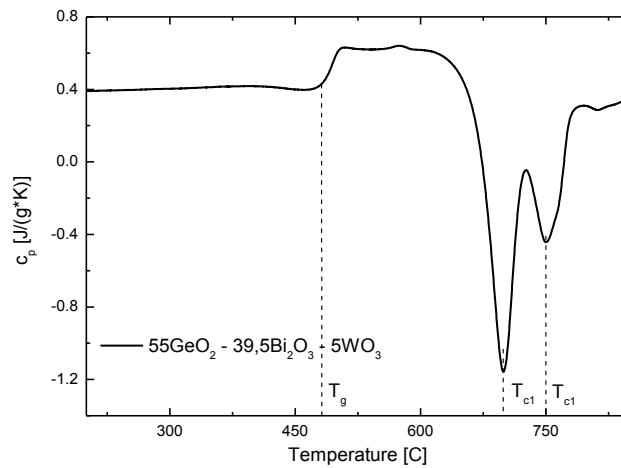

Figure A.8: Determination of glass transition temperature and crystallisation temperature from c_p -measurements (heat capacity) of a 55 GeO_2 – 39,5 Bi_2O_3 – 5 WO_3 glass.

To explore extrusion of the bismuth-germanate glass system, we commenced with the glass composition 70 GeO_2 – 24.5 Bi_2O_3 – 5 WO_3 – 0.5 CeO_2. We prepared a glass billet of ~3cm diameter and ~4cm height from a 150g batch. The glass billet was extruded into a rod of 10mm diameter (Fig. A.9). Although the glass billet showed a few bubbles, no defects were visible in the extruded rod. Unfortunately due to a gradient in the radial temperature profile within the extrusion furnace, the rod showed severe bending. However, this can be prevented in the future by repositioning the extrusion furnace.
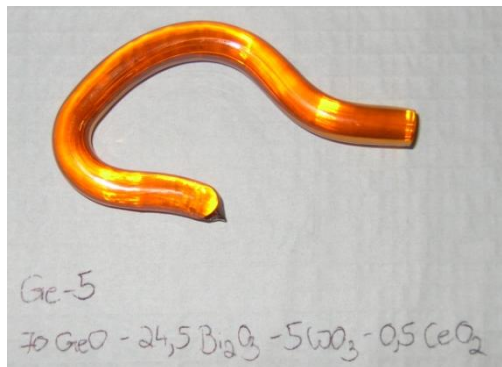
Figure A9: Extruded rod using 70 GeO_2 – 24.5 Bi_2O_3 – 5WO_3 – 0.5CeO_2 glass billet.

Raman spectroscopy showed that the maximum phonon energy of the bismuth glasses is with 920cm^{-1} (Fig. A.10) relatively high among germanate glasses. Although crystal-free glasses could be fabricated in quantities up to 100g, detailed crystallisation investigation revealed that bismuth germanate glasses

23

demonstrate surface crystallisation in the temperature window for fibre drawing, making the glass less suited for fibre fabrication.
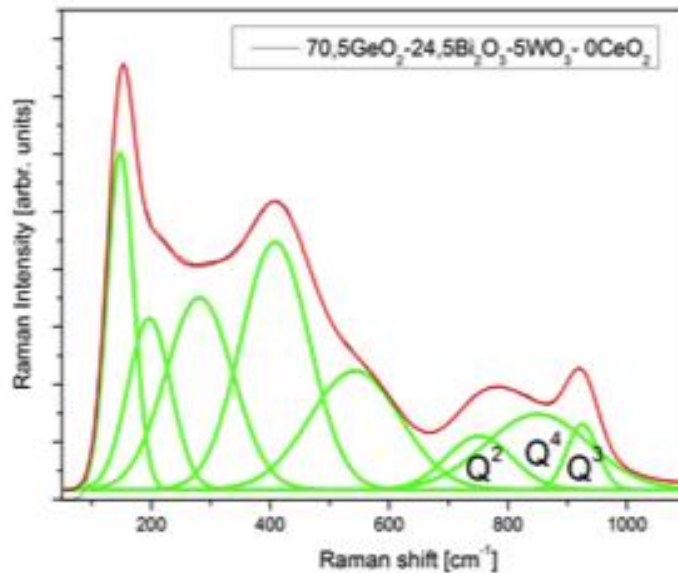

Figure A.10: Raman spectrum of the 70.5 GeO$_2$ – 24.5 Bi$_2$O$_3$ – 5 WO$_3$ glass without CeO$_2$ addition.

(c) Lead-germanate glasses developed in-house

We fabricated a range of lead germanate glasses with varying La$_2$O$_3$ and Na$_2$O content (Fig. A.11). Na$_2$O was added as for lead-silicate glasses, small amount of Na$_2$O prevents devitrification [5]. Addition of La$_2$O$_3$ was also explored as this component increased the glass stability of tellurite glasses and allows rare earth doping without changing the glass properties [6]. In contrast to bismuth germanates, the lead germanate glasses did not form heavy metal nanoparticles due to reduction of heavy metal ions (i.e. bismuth or lead) during glass melting, which is advantageous regarding reproducible glass quality.
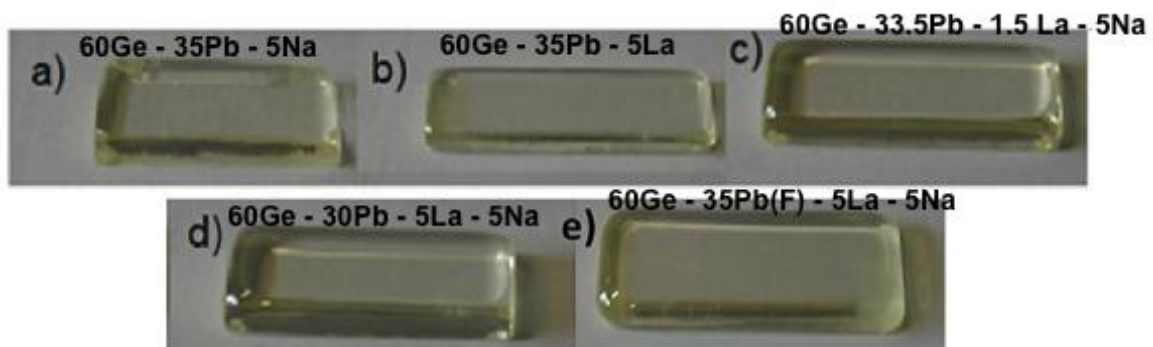
Figure A.11: Lead-germanate glasses of different compositions.

Using 30g batches, systematic variation of the melting temperature and time demonstrated that at least 1h melting time at 1250°C is required to dissolve all raw materials and obtain a clear glass melt. Both the

Na-containing and the Na-free glasses could be doped with up to 2 mol% Tm_2O_3 (~4wt% Tm_2O_3) without crystallization.

Raman spectroscopy showed that the maximum phonon energy of lead germanate glasses is with 830cm^{-1} (Fig. A.12) significantly smaller compared with bismuth germanate glasses. The lower phonon energy offers negligible nonradiative multiphonon relaxation of rare earth transitions up to 2.5µm emission wavelength.
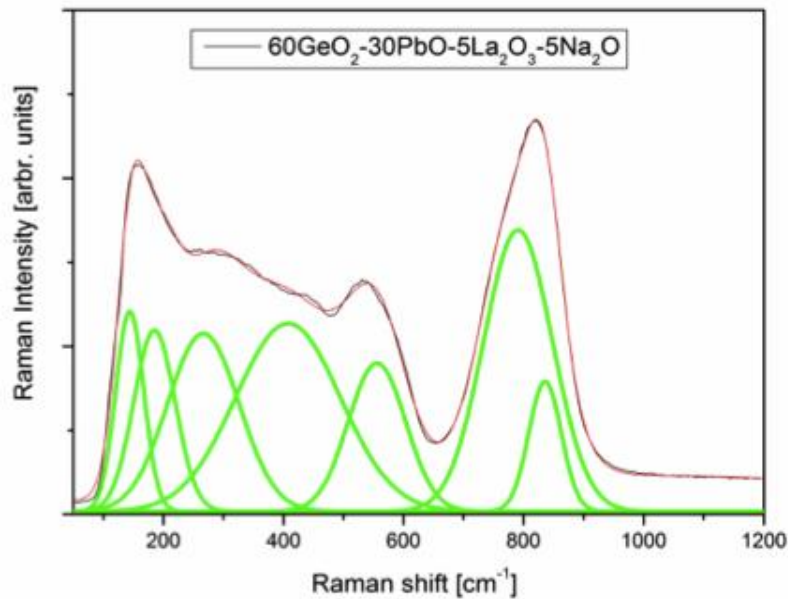

Figure A.12: Raman spectrum of a lead-germanate glass.

To determine the position of the IR edge and the OH content (i.e. intensity of the OH absorption band at ~3µm wavelength), we prepared polished glass plates and measured the FTIR spectra. As shown in Figure A.13, all three germanate glasses show intense water absorption band at 3µm due to melting in ambient atmosphere. The IR edge of the two in-house lead-germanate glasses is located at ~5.5µm, which agrees with the small phonon energy of 830cm^{-1} for lead-germanate glasses. This promises the development of high-efficiency Tm^{3+} fiber lasers at ~2µm. As noted above, the IR edge of commercial bismuth-germanate glass is shifted to shorter wavelength due to SiO_2 content in the glass.

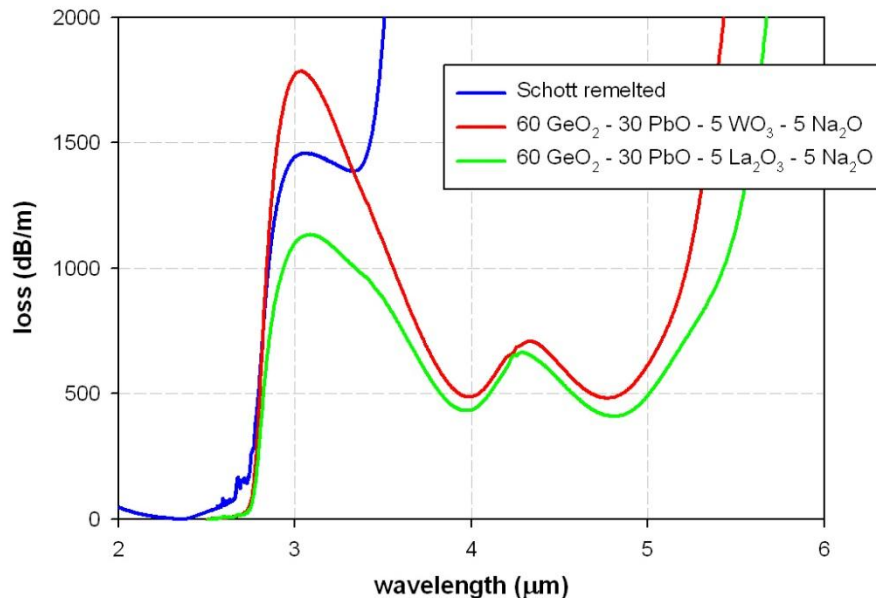*Figure A.13: FTIR spectra of lead-germanate glasses showing the OH-absorption peak at 2.9 µm and the IR edge at ~3.5µm for the Schott glass and at ~5.5µm for lead-germanate glasses.*

All germanate glasses were melted in open air thus far, resulting in relatively high water content and thus absorption at ~3µm. Na-free glasses exhibit a lower OH content (i.e. peak absorption at 3µm) compared with Na-containing glasses melted using the same conditions (Fig. A.14). For 30g glass batches and 0.5-3h melting time, Tm-doping increased the OH content (Figs. A14 and A.15). In order to reduce the water content we investigated partial replacement of PbO with PbF_2. For longer melting time of 3h, 5mol% PbF_2 showed a significant reduction in the OH content (Fig. A14). For shorter melting times of 0.5h, 10 mol% PbF_2 was required to achieve a considerable reduction in the water content (Fig. A.15). However, for long melting time of 5h, the water content increased compared with shorter melting time (Fig. A15), and for 10h melting time the water content was similar to that of glasses made from PbF_2–free glass batches. The increase in water content is attributed to evaporation of the fluoride from the glass melt, thereby approaching the same equilibrium between water in the glass melt and the atmosphere above the glass melt. This demonstrates that use of fluoride requires careful optimization of the fluoride content, melting time and temperature.
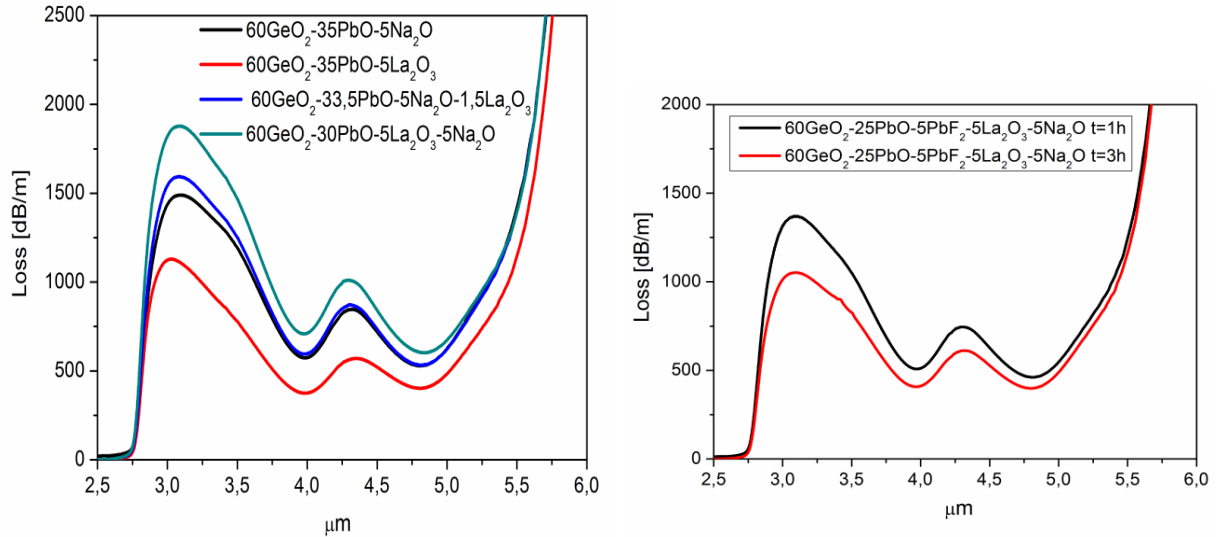
Figure A.14: FTIR spectra of different lead-germanate glass samples melted from 30g batches at 1250°C for 30min (left) or for 1-3h (right).
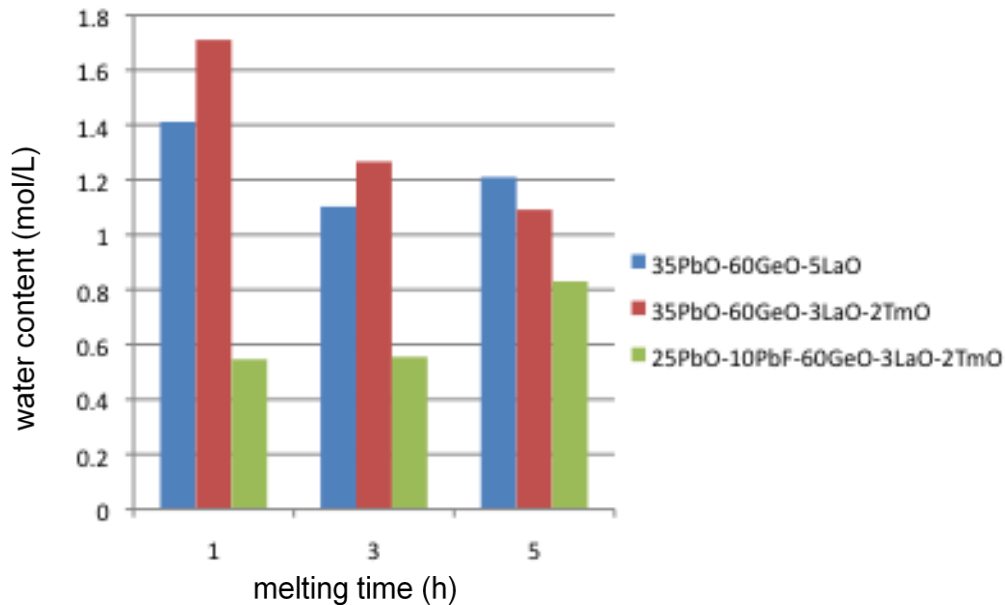

Figure A.15: Water content (determined using the peak OH absorption at 3µm) for lead-germanate glass samples melted from 30g batches at 1250°C for different melting times.

Both Na_2O-containing and Na_2O-free lead germanate glasses were successfully extruded into defect-free rods (Fig. A.16). In addition, feasibility of extrusion of a structured preform was demonstrated (Fig. A.17). From the rods and the preforms, fibres were drawn and the fibre loss in the visible to near-infrared region was measured using the cut-back technique. For Na_2O-containing glasses, shorter melting time of 3h for the billet from which the fibre was made resulted in surface crystallization, which led to high fibre loss (e.g. 8.4dB/m at 790nm). Increased melting time of 5h, reduced the fibre loss to 1.2dB/m at 790nm (Fig. A.18). The lowest loss could be obtained for Na_2O-free lead germanate fibres.

The undoped fibre exhibits a minimum loss of 0.2dB/m at 1250nm and 0.6dB/m at the pump wavelength of 790nm.

Figure A.16: (Left) 3cm diameter lead-germanate glass billet made from 150g batch and (Right) extruded rod of 1cm diameter and 16cm length made using this billet.
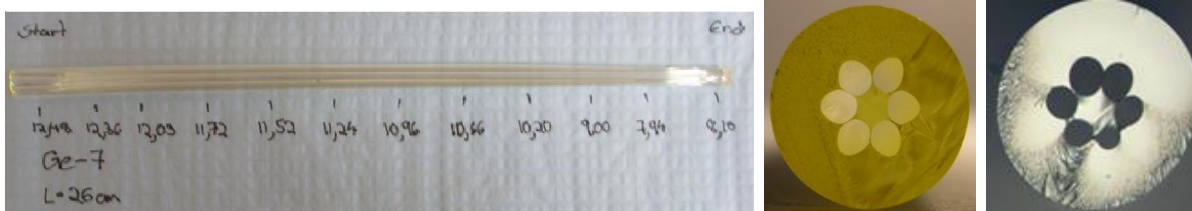

Figure A.17: (Left) Extruded lead-germanate glass preform of ~1cm diameter and 26cm length, (Middle) cross-sectional view of the preform, and (Right) cross-sectional view of the fiber.
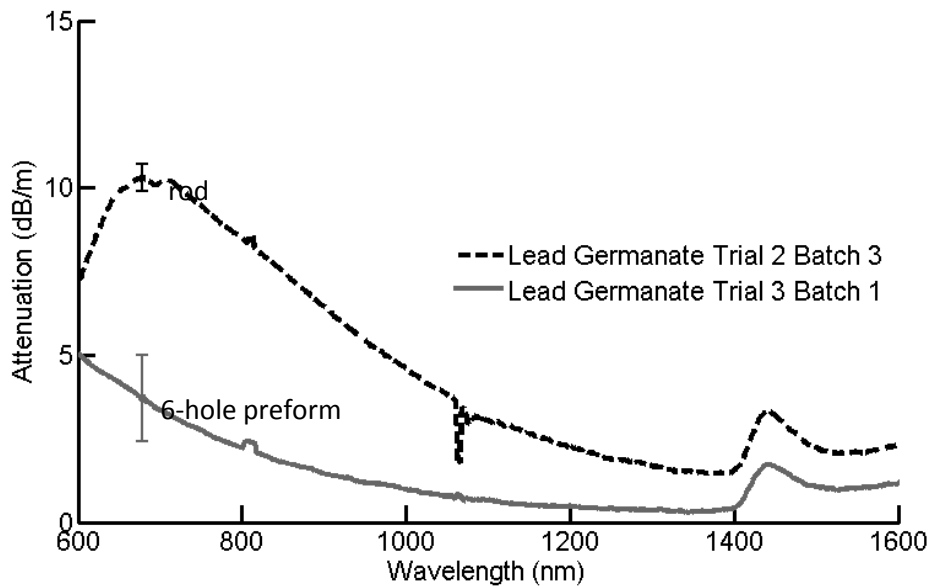

Figure A.18: Na$_2$O-containing germanate glass fibres: Propagation loss for the fibers made from the extruded rod (Trial 2) and the extruded 6-hole preform (Trial 3). The melting time of the billets used to fabricate fibers Trials 2 and 3 was 3h and 5h, respectively.

(1) Germanate glass based fibers

- We investigated the feasibility of using the extrusion technique for the fabrication of preforms from germanate glass with high softening temperature. We used the commercial germanate glass BZT (Kigre Inc.) for this investigation. We successfully extruded a 10mm diameter rod and a structured preform with suspended core (Fig. B.1). Both the rod and the preform were crystal-free and exhibited good optical quality.
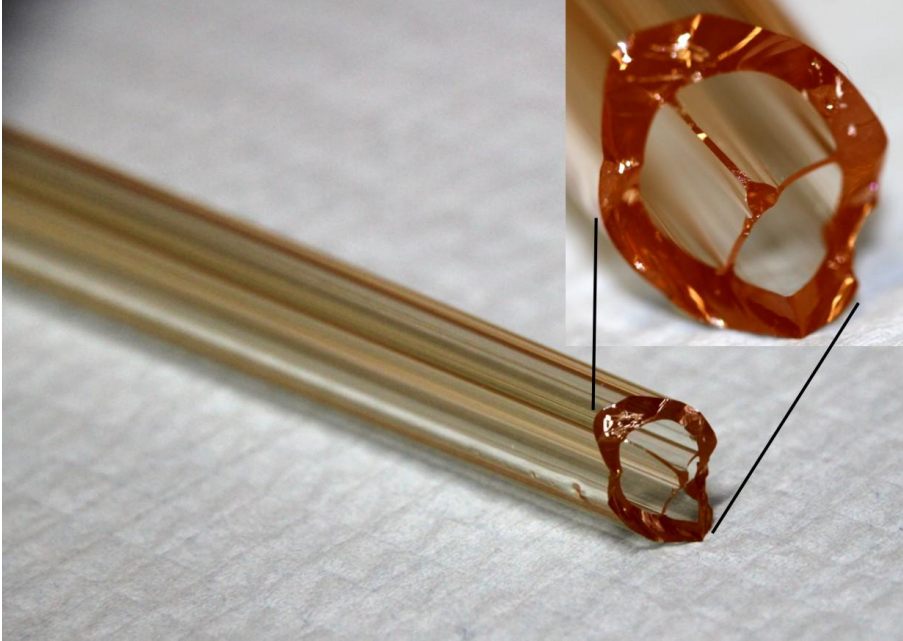

Figure B.1. Photograph of extruded structured preform made at IPAS from BZT germanate glass.

- Using our glass flow model, the experimentally determined extrusion force values at different extrusion temperatures was determined. The temperature-viscosity behaviour of the BZT germanate glass and the two in-house developed lead-germanate glasses (GPL and GPLN) was calculated. From the temperature-viscosity curves we calculated the softening temperatures of the germanate glasses. The softening temperature of the BZT glass is ~800°C, whereas the softening temperature of in-house lead-germanate glasses is in the range 530-550°C.

- The extruded BZT rod was drawn down to a bare, unstructured fibre with 160 µm outer diameter. The loss of the fibre was measured using the cutback-technique. The BZT glass demonstrates comparable minimum loss of ~1dB/m compared with in-house lead-germanate glass fibres (Fig. B.2). In contrast to the lead-germanate glass fibres, the BZG glass fibre does not show the OH vibration overtone absorption at 1.45µm. This result is consistent with bulk glass loss measurements (Fig. B.3) in the mid-infrared. The lead-germanate glasses used for fibre fabrication were melted in open air and therefore contain a larger amount of OH groups, resulting in high absorption of the fundamental OH vibration at 3µm. The BZT glass exhibits a considerable lower OH absorption, which correlates with the absence of the overtone absorption at 1.45µm. Note that lead-

germanate glasses melted in dry atmosphere show also low OH absorption as the BZT glass, promising low absorption >1.4µm.
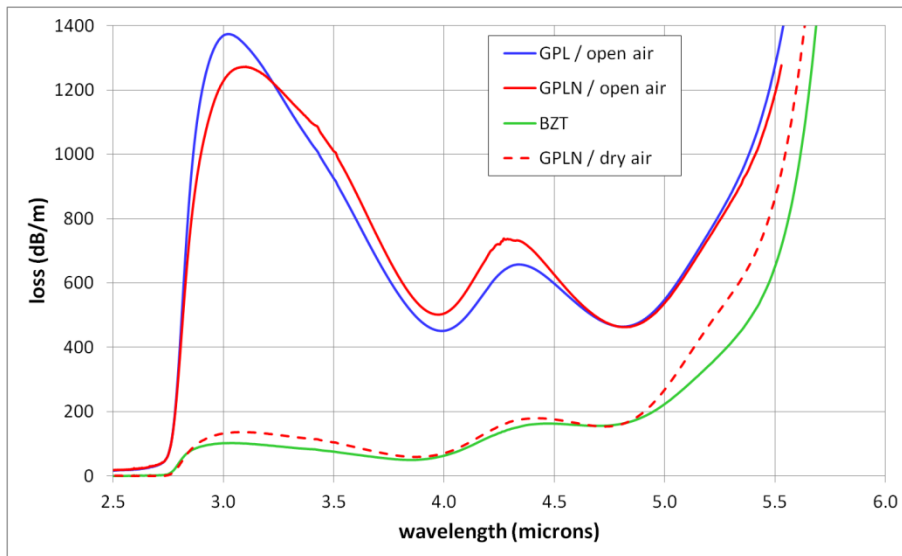

Figure B.2. Bulk glass loss spectra of polished germanate glass plates.
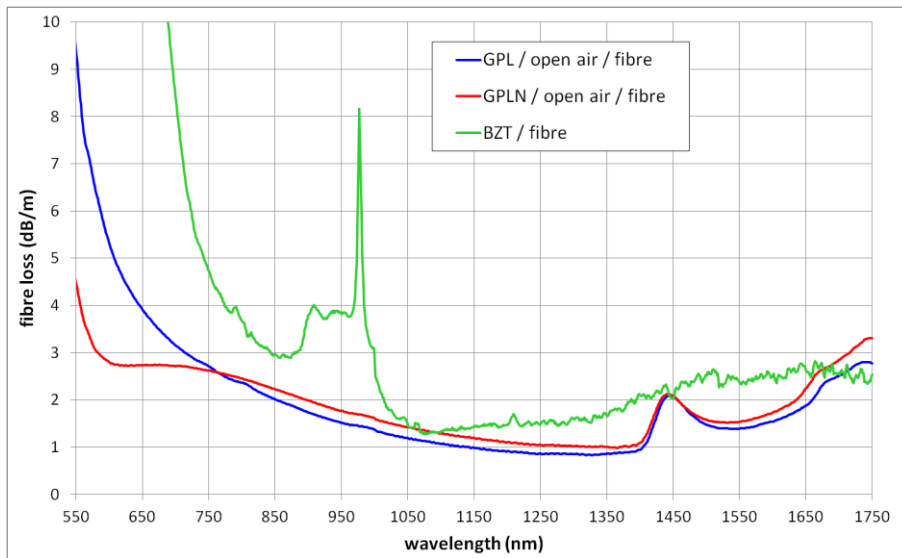

Figure B.3. Fibre loss spectra of unstructured germanate glass fibres.

(2) Rare earth doped germanate fiber laser development

In this stream we achieved fabrication of a 'proof of concept' for a unique microstructured holmium doped active fibre for use as a 2.1 μm laser. The laser and pump laser characteristics targeted were:

- *Ho^{3+} emission transition $^5I_7 - {}^5I_8$ at 2.1μm*
- *Pump source: Tm-silica fibre laser at 1.9μm*

Stage 1 focussed on the identification of germanate glass compositions suitable for drawing of low-loss fibres. To reduce risk we:

- Developed low-softening temperature germanate glasses fabricated in-house

AND

- Optimised our extrusion fabrication techniques to high-softening temperature commercial germanate glass

- Several glass systems investigated experimentally:

60 GeO_2 – (35-x) PbO – x La_2O_3 – 5 Na_2O [x = 0, 1.5, 5]

60 GeO_2 – (35-x) PbO – 5 La_2O_3 – x Na_2O [x = 0, 5]

70 GeO_2 – 25 Bi_2O_3 – 5 WO_3

- With the most suitable composition identified as:

60 GeO_2 – 35 PbO – 5 La_2O_3

- We then fabricated crystal-free glass billets up to 150g (sized for fibre fabrication, Fig C.1)
- Ho^{3+} doping achieved via substitution of passive rare earth La_2O_3 (Fig. C.2)
- We measured similar bulk loss for commercial & in-house glass
- Commercial glass offers higher thermal stability & requires high temperature extrusion
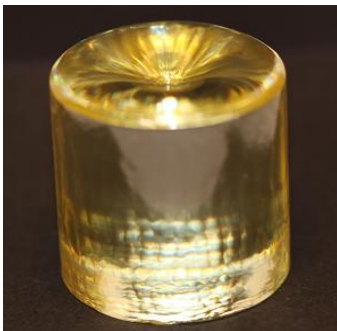

| *Fig. C.1 Billet of undoped germanate fabricated at IPAS* | *Fig. C.2 Spectroscopic sample of holmium doped germanate glass* |

- To make lasers between 2-5 μm it is vital to minimize the water content of the glass (see Fig B.3 and Fig. C.3).
- To this end we developed an effective dehydration method. This involved melting the raw materials in a high purity and dry glovebox using a newly commissioned (and highly customized) high temperature (1250°C) controlled atmosphere glass melting capability. This has resulted in our in-house glass possessing comparable losses with commercial glass.
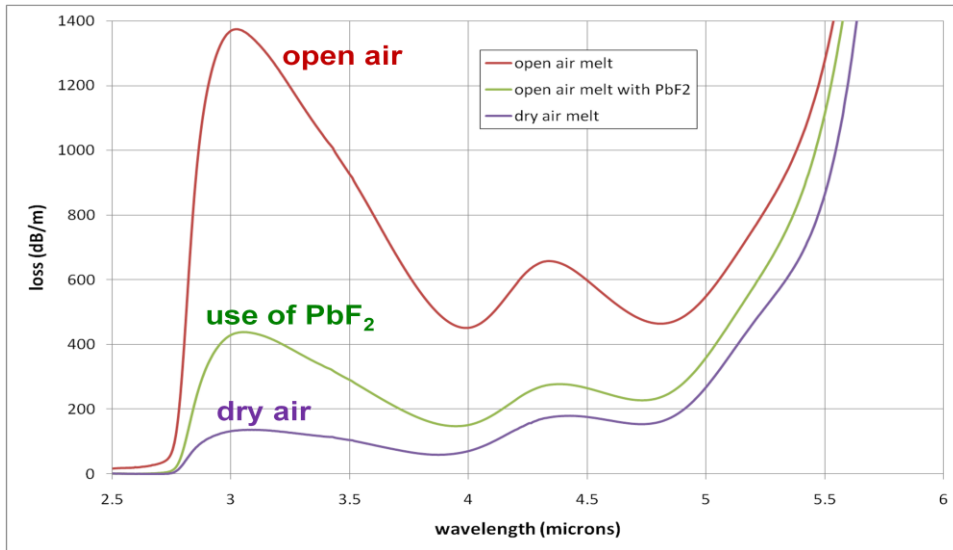

Fig. C.3 Measured losses (FTIR) of bulk germanate glasses fabricated in (1) open air (2) dry air (and with the addition of PbF$_2$). Nb. Due to small samples the loss near ~2 μm can't be measured in bulk glass using this technique.

(3) Spectroscopic characterization of Ho-doped germanate glass

In earlier work, we fabricated Ho-doped GPL glass with ion density of 0.95×10^{20} Ho^{3+} cm^{-3} and measured the absorption of Ho^{3+} in this glass. In this work we conducted Judd-Ofelt analysis of the absorption spectrum in order to calculate radiative lifetimes and branching ratios of the various emission transitions. Fig. D.1 shows the experimental and calculated oscillator strengths of the various absorption transitions. The experimental oscillator strengths were determined from the measured integral absorption cross sections. Using these oscillator strengths, the Judd-Ofelt parameters were calculated. The Judd-Ofelt parameters were then used to calculate oscillator strengths, radiative lifetime and branching ratios of the various transitions (Fig. D.1). The good agreement between experimental and calculated oscillator strengths (Fig. D.2) demonstrates the validity of the Judd-Ofelt analysis for our Ho-doped GPL glass.

The transition of interest of this work is the $^4I_7 \rightarrow {}^4I_8$ transition with emission at ~2μm. The radiative lifetime of this transition is 7.8ms. Using the data provided in Ref [1], we calculated the non-radiative decay from the $^4I_7$ excited state due to multiphonon relaxation for germanate glass. Using this value, we predicted the fluorescence lifetime to be approximately ~6.1ms, corresponding to a quantum efficiency of 78%. Compare the quantum efficiency of Ho-doped silica fibre was reported to be only ~10% [2]. The significantly higher quantum efficiency of Ho^{3+} in germanate glass relative to silica is due to the considerably lower phonon energy of our gemanate glass (~830cm^{-1}) compared with silica (~1100cm^{-1}).
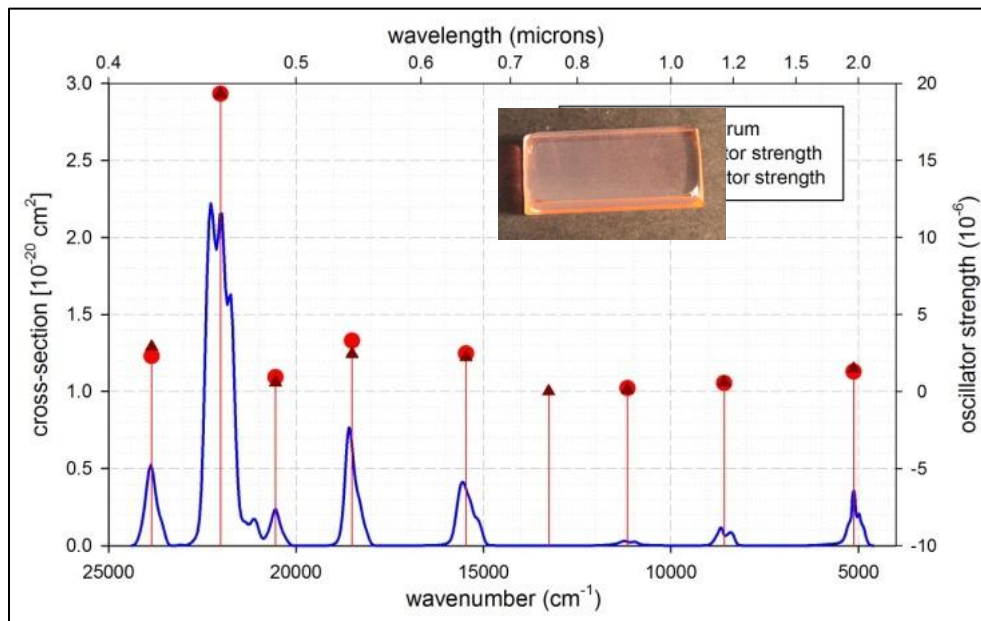

Fig. D.1: Spectrum of the absorption cross section of Ho^{3+} in GPL glass. The experimental and calculated oscillator strength for each absorption band is shown.
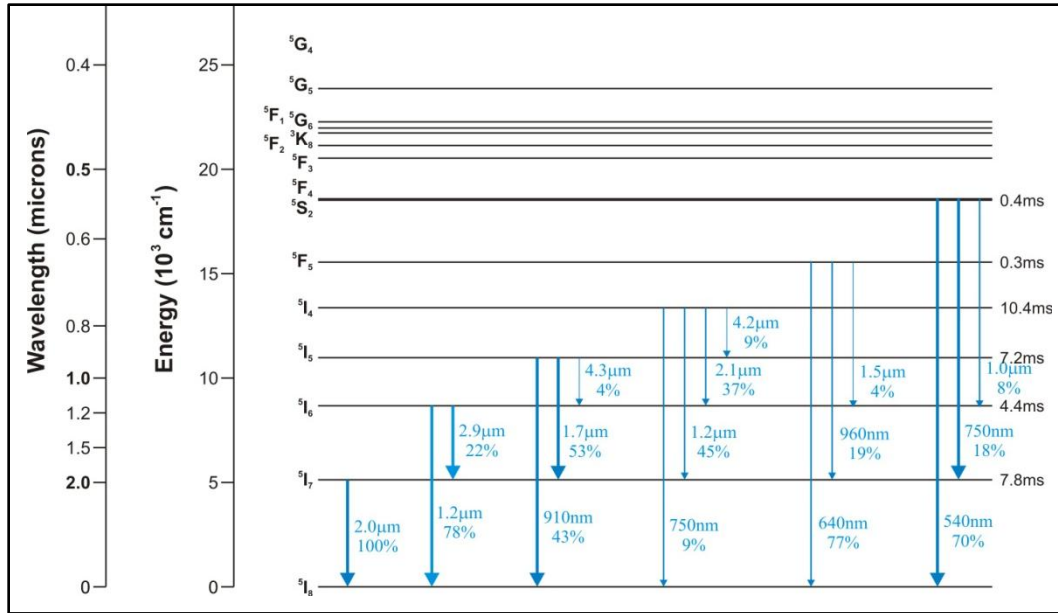
Fig. D.2. Energy level diagram of Ho^{3+} in GPL glass. The values in ms are the radiative lifetimes. The values in % are the branching ratios for the various transitions originating from an excited state. The values in nm and μm designate the calculated wavelengths of the various emission transitions.

[1]   J.M.F. van Dijk, M.F.H. Schuurmans, "On the nonradiative and radiative decay rates and a modified exponential energy gap law for 4f–4f transitions in rare-earth ions," J. Chem.. Phys. **78**, 5317-5323 (1983).

[2]   B. Samson, G. Oulundsen, A. Carter, S.R. Bowman, "OPTICAL FIBER FABRICATION: Holmium-doped silica fiber designs extend fiber lasers beyond 2 μm," Laser Focus World, 8 Jan 2012

(4) Recent germanate glass melting and extrusion results (2013)

Nb. In early 2013 the new Braggs laboratories were completed, and all glass fabrication transitioned to this facility over the first 6 months of 2013.

<u>Glass melting</u>

Towards the end of 2013, two large billets (180g) of GPNL5 glass were made successfully in the oxide glovebox (KGe020 and KGe021) in the new Braggs facility. The FTIR spectra of the billets together with a small GPNL5 melt made in the physics building (KGe001) are shown in Figure E.1. The significantly reduced OH absorption at ~3µm for KGe020 and KGe021 (despite large melt size) is attributed to the lower water content/dew point of the nitrogen in the Braggs building (<0.1ppm$_v$/-99°C) compared to the nitrogen in the Physics building (10ppm$_v$/-60°C).
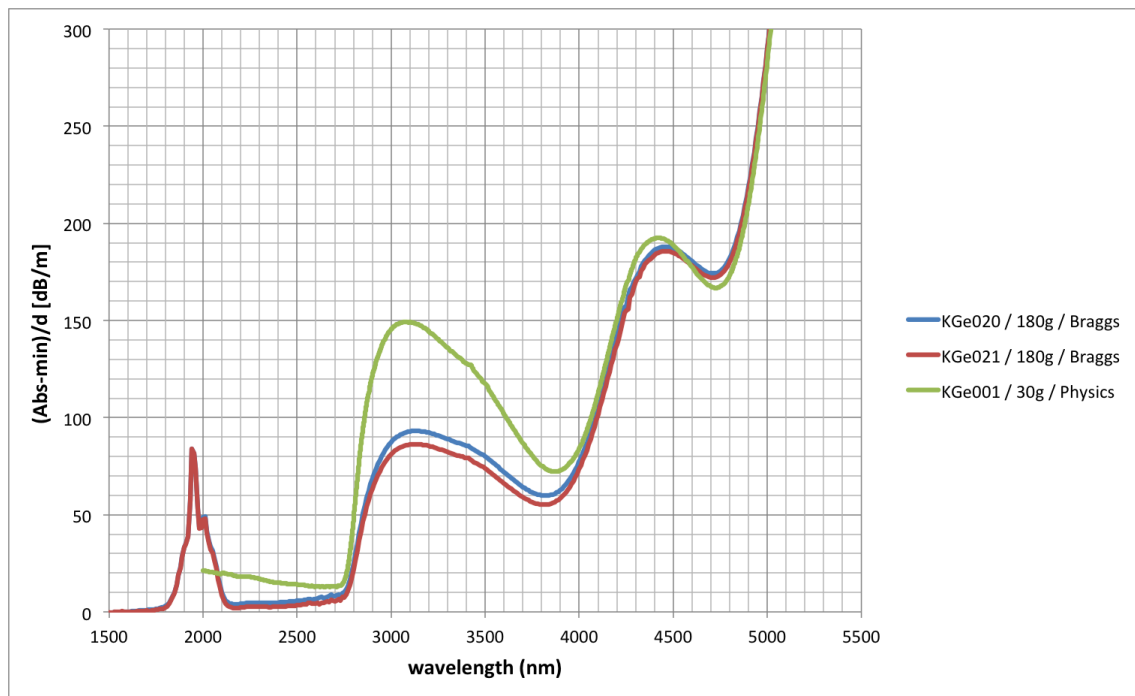

Figure E.1: FTIR spectra

The two billets were doped 0.2wt% Ho. As no Ho_2O_3 was available, we used HoF_3 as raw materials for the doping assuming that HoF_3 is completely converted to Ho_2O_3 as follows.

$$2\ HoF_3 + 3/2\ O_2 \rightarrow Ho_2O_3 + 3/2\ F_2$$
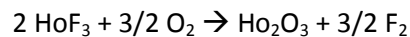
However, we do not know if dry oxygen is sufficient to provide complete conversion. Recently, we have acquired Ho_2O_3 raw material, which will be used for future melts. Assuming complete conversion to Ho_2O_3 and using density of 5.83 g/cm^3 as measured for small glass samples of GPNL5, the Ho ion density for the two billets was calculated to be 0.43×10^{20} Ho^{3+} cm^{-1}. Using this concentration and UV-Vis-NIR

glass spectra of the two billets, we calculated the absorption cross sections of the Ho^{3+} bands (Figure E.2).
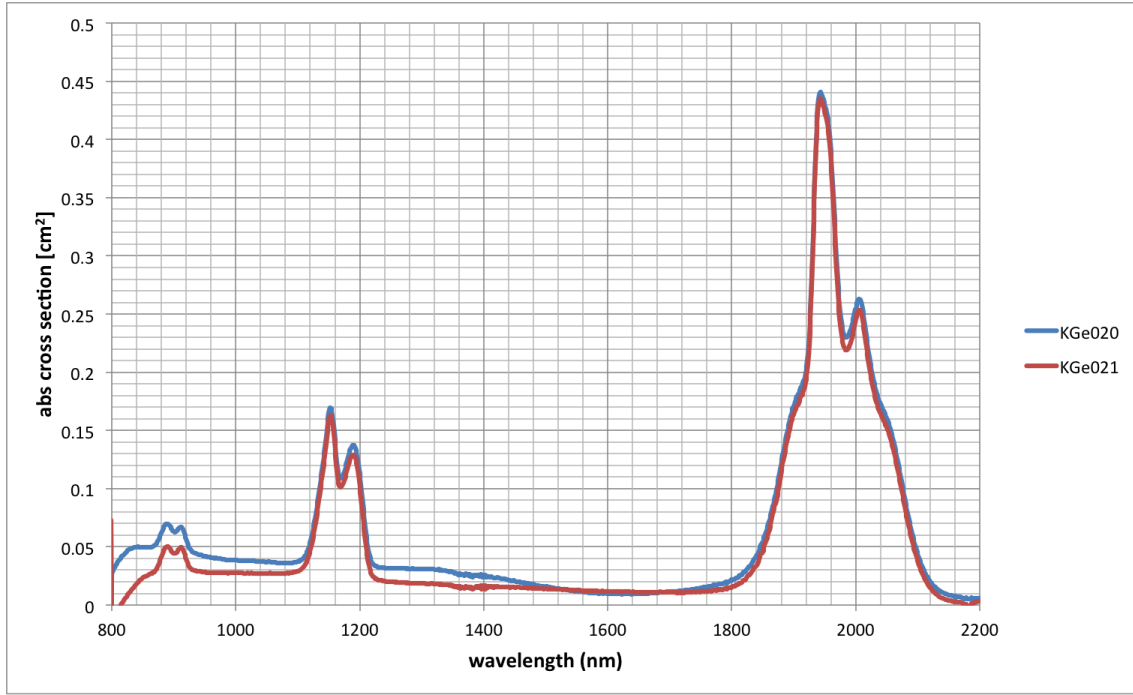
Figure E.2: Absorption cross section spectra of Ho^{3+} bands

For future trials we need to address the following issues:

a) The $1250^{\circ}C$ melting temperature for prolonged time (5h or longer) results in severe surface crystallization of the silica liner, which will limit the number of melting trials that can be made per liner. In addition, the surface crystallization results in flakes coming off the liner, which enhances the risk of getting particles and thus scattering centres into the glass. The high loss of the germanate WW fibre published in [1] is attributed to particles from the liner being incorporated into the melt.

b) We observed germanate glass in the crucible stand. We assume this is the result of vigorous release of CO_2 from the Na_2CO_3 used for batching at the high melting temperature of $1250^{\circ}C$ combined with large filling of the crucible. We will investigate release of CO_2 (and water) at low temperature of $500^{\circ}C$. Hopefully at $500^{\circ}C$, the batch is still in powder form so that the batch can be added to the melting crucible in tow steps as done today. Note that we use currently 100mL Pt crucible for melting 180g batch, which is not ideal but we had problems with the 200mL crucible sticking to the stand. In hindsight, the sticking might be a results of the batch/glass spillage due to CO_2 release. Once we figures out how to release CO_2 at low temperature, we can look into usage of 200mL crucible.

Tellurite glass melted using 100% dry oxygen atmosphere exhibited ~7 times higher OH loss at 3.3 μm than corresponding glass melted in 80% N_2 / 20% O_2 dry atmosphere. This difference in loss suggests that O_2 gas used for melting has considerably higher water content. However, dew point measurements of the O_2 and N_2 line today resulted in similar and low dew points of -99°C (<0.1ppm$_v$ water) for N_2 and -89°C (~1ppm$_v$ water) for O_2. Further work is required to determine the impact of pure oxygen atmosphere on OH content in glass. In addition, we need to determine the water content of the gases once purged through the furnace liner. Note that we have gas purifier in stock in case we need to dry gases just before entering the furnace liner. It might be worth exploring the use of 100% oxygen atmosphere on the fibre loss. According to preliminary absolute absorption measurements, the absorption of our glasses is only 0.2 dB/m at 1.2 μm, whereas the loss of unstructured, extruded GPNL5 fibre was measured to be ~1 dB/m at 1.2 μm, demonstrating significant contribution of scattering loss. Small amount of Pb^0 particles and/or Pt^0 particles could contribute to scattering loss. 100% oxygen atmosphere might prevent formation of any metal particles such as Pb^0 and Pt^0.

We also fabricated a 0.4 wt% holmium doped germanate sample, and measured the holmium absorption as a preliminary step to fabrication of a holmium doped germanate microstructured fibre. The measured absorption is shown (Fig. E.3) of our in-house manufactured germanate glass to produce a microstructured preform (for a holey fibre) which was then drawn down to fibre as shown in Fig. E.6., with a holmium ion absorption of 1.5 dB/cm at 1945nm ($^5I_7 - {}^5I_8$) .
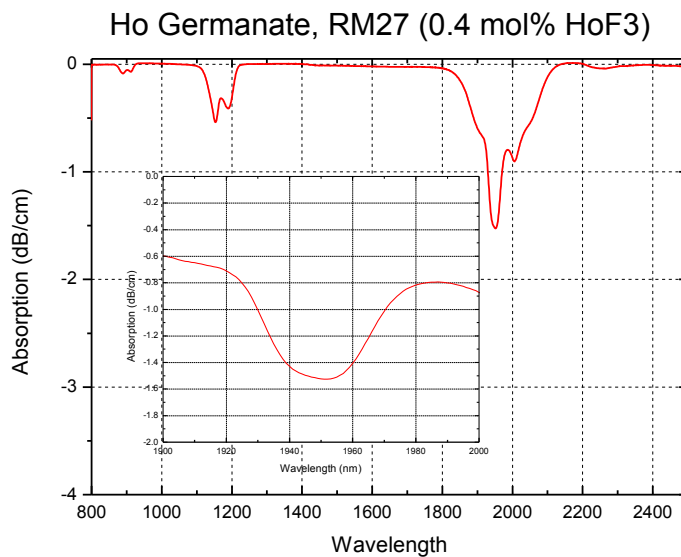

Fig. E.3 Measured absorption of holmium doped germanate glass fabricated at IPAS.

Extrusion

The two billets KGe020 and KGe021 were extruded into preforms with 4 rings of holes (Ge-25 and Ge-26 preforms). A photograph of the cross section of the preform made from KGe020 at ~1cm from start of extrusion is shown in Figure E.3, together with the cross sectional photograph of a 3-ring preform made from GPL5 glass some time ago. 4-ring dies (in stock) having each a central pin were modified such that the central pin was removed and replaced with a feed hole. Due to this modification, the central feed hole was slightly larger than the other feed holes, resulting in enhanced flow in the centre and thus some distortion of the holes in the inner ring. The new dies had d/Λ ratio of 0.7, whereas the previously used 3-ring dies had d/Λ ratio of 0.5.
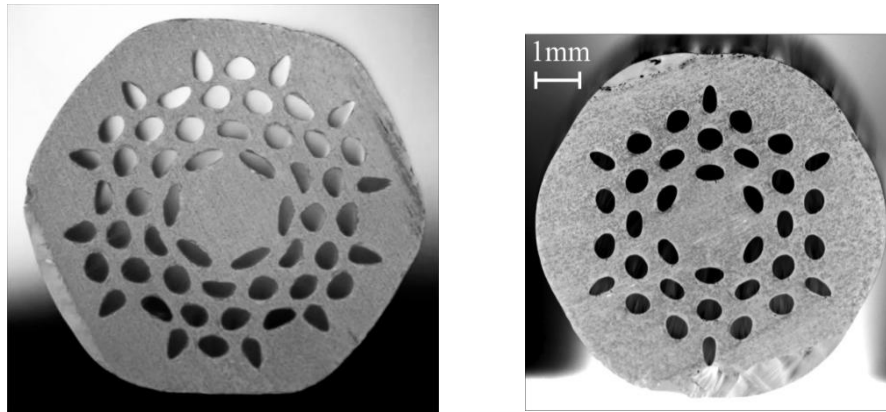

Figure E.4: Cross-sectional images of extruded germanate preforms: (Left) preform made from GPNL5 billet KGe020 using die with d/Λ=0.7 and die exit diameter of 17.8mm, (Right) preform made from GPL5 glass using die with d/Λ=0.7 and die exit diameter of 15.5mm.

In future work we will optimize the dies/structures we use. 3-ring dies have the advantage that they result in thinner and thus longer preforms. Larger d/Λ ratio will reduce the amount of pressure required to keep the holes open during fibre drawing.

- We have also demonstrated extrusion fabrication (Fig. E.4) of our in-house manufactured germanate glass to produce a microstructured preform (for a holey fibre) which was then drawn down to fibre as shown in Fig. E.6

- The measured fiber loss of the un-doped germanate fibers is shown in Table E.1 compares loss of structured vs unstructured fibers.

- More recently we achieved fabrication of a holmium doped germanate glass fiber (OD~160 μm), designed for large mode operation at 2.1 μm (Fig. E.7) . Characterisation of this fiber is still ongoing. Preliminary results indicated that loss is currently high (> 10 dB/m) due to possible crystalisation due to impurities in the glass (impure RE dopant used). Future work will eliminate these possible impurities.

- After significant experimentation on in-house germanate, we have determined that lead-germanate glass $GeO_2 – PbO – La_2O_3 – Na_2O$ (GPLN)) is the most suitable compositions for fiber fabrication.
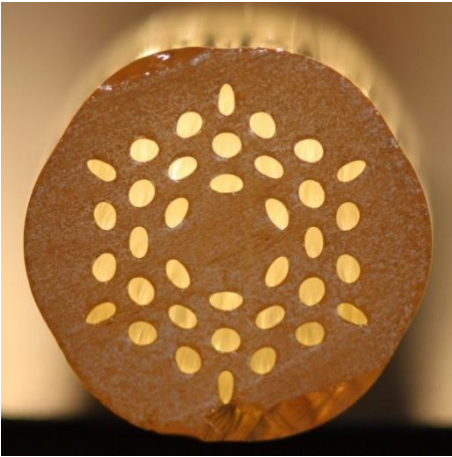
Figure E.5: Extruded un-doped germanate glass preform
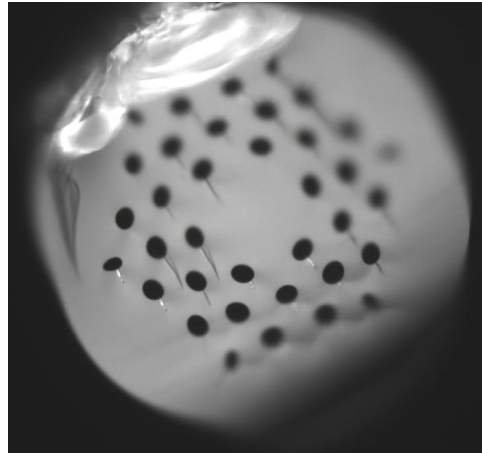
Figure E.6: Germanate microstructured fiber drawn from the preform shown in Fig. E.4 Core diameter is ~ 20 μm.

Unstructured germanate fiber:	0.3 dB/m at 1.4μm
microstructured germanate fiber:	4.4 dB/m at 1.4μm
microstructured germanate fiber:	5.0 dB/m at 2.0μm

Table E.1: Measured germanate fibre losses at 1945nm for a solid fibre and a microstructured fibre.
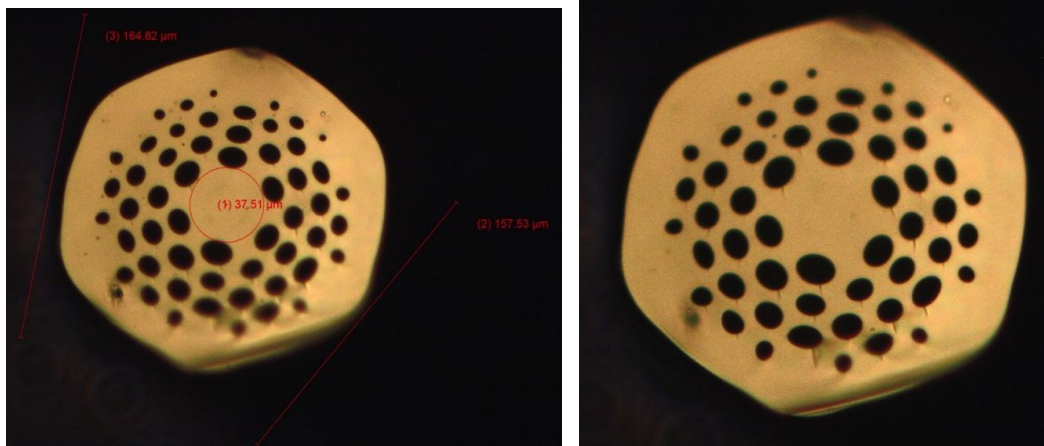
Figure E.7: 0.4 wt % holmium doped germanate preform drawn to fiber, OD~160μm (IPAS glass, extrusion and drawing).

(5) Conclusion:

Over the last few years, the IPAS team have made strong progress towards developing a completely vertically integrated capability in fabricating and testing microstructured germanate fiber lasers. To the best of our knowledge this is a unique capability, and we believe we are well placed to demonstrate this new class of high power capable short/ mid infrared germanate fiber lasers. This research is both novel and challenging as it involves developing complex microstructured features in a relatively immature glass (especially when compared to silica), whilst maintaining low-loss, and testing the design as a laser in the short to mid-infrared which is one of the hardest spectral regions to operate a laser.

Relevant papers published for this AOARD grant.

1.   H. T. Munasinghe, A. Winterstein-Beckmann, C. Schiele,D. Manzani, L. Wondraczek, S. Afshar, T. M. Monro, H. Ebendorff-Heidepriem, "Lead-germanate glasses and fibers- a practical alternative to tellurite for nonlinear fiber applications" Optical Materials Express, 1488-1503, (2013)
2.   "Tandem-pumped, Air-clad, Holmium-doped Silica Fibre Laser Optimization", S.W.S. Ng, D.G. Lancaster, D.J. Ottaway, P.C. Henry, R.Kosteki and T.M. Monro, submitted to Photonics West 2013.
3.   "Air-clad Holmium-doped Silica Fibre Laser", S.W.S. Ng, D.G. Lancaster, D.J. Ottaway, P.C. Henry, R.Kosteki, and T.M. Monro, Submittted to the Australian Conference on Fibre Technology, 2012.
4.   "Power scaling of short-wave infrared fibre lasers", S.W.S. Ng, D.G. Lancaster, D.J. Ottaway, T.M. Monro, Oral paper at Frontiers in Optics Conference. Rochester, 2012.
5.   "Tandem-pumped, air-clad holmium doped silica fiber laser", S.W.S. Ng, D.G. Lancaster, D. J. Ottaway, T.M. Monro, manuscript under preparation, to be submitted to Optics Letters.
6.   A. Winterstein, S. Manning, H. Ebendorff-Heidepriem, L. Wondraczek, "Luminescence from bismuth-germanate glasses and its manipulation through oxidants," Optical Mat. Expr., **2**, 1320-1328, 2012.
7.   Heike Ebendorff-Heidepriem, Christian Schiele, Anja Winterstein, Lothar Wondraczek, David G. Lancaster, David Ottaway, and Tanya M. Monro, "New Germanate Glasses For Infrared Fibre Applications," submitted to Australian Conference on Optical Fibre Technology, Sydney, Dec 2012